

Sukkur IBA **Journal** of Emerging Technologies

P-ISSN: 2616-7069

Volume: 2 | No.: 1 | Jan - June | 2019

Sukkur IBA Journal of Emerging Technologies (SJET) is the bi-annual research journal published by **Sukkur IBA University**, Pakistan. **SJET** is dedicated to serve as a key resource to provide applied engineering research associated with the Electrical, Electronics and innovations in Energy at the global scale. This Journal publishes manuscripts which are well written by highlighting development in emerging technologies. This Journal covers all branches of Engineering, Science & Emerging Technologies.

Copyright: All rights reserve. It is restricted to publish any part of the publications produced, translated or stored in retrieval system or transmitted in any form or by any means, electronic, mechanical, photocopying and/or otherwise the prior permission of publication authorities.

Disclaimer: The research material expressed in **Sukkur IBA Journal of Emerging Technologies (SJET)** is sole contribution of the authors. The research contribution of the authors does not reflect the management, advisory board, the editorial board, **Sukkur IBA University** press and the organization to which the authors are affiliated. Manuscripts published in **SJET** shall be processed through double-blind peer-reviewed by the two experts of field. The identities of the experts/reviewers shall remain anonymous to the authors. The Journal shall be published in June i.e. once a year. Neither the **Sukkur IBA University** nor the **SJET** shall be responsible for errors or any consequences highlighted by the reader. The errors and deficiencies in terms of research in manuscript can directly be reported to the authors.

Publisher: **Sukkur IBA Journal of Emerging Technologies (SJET)**
Office of Research, Innovation & Commercialization – ORIC
Sukkur IBA University - Airport Road Sukkur-65200, Sindh Pakistan

Tel: (09271) 5644233 -37 Fax: (092 71) 5804425 Email: sjet@iba-suk.edu.pk URL: sjet.iba-suk.edu.pk

Mission Statement

The mission of **Sukkur IBA Journal of Emerging Technologies (SJET)** is to provide a premier interdisciplinary platform to researchers, scientists and practitioners from the field of engineering in particular, electrical, electronics, renewable and emerging engineering fields for dissemination of their finding and to contribute in the knowledge domain.

Aims & Objectives

Sukkur IBA Journal of Emerging Technologies (SJET) will publish and encourage the submission of critically reviewed manuscripts on the cutting edge research in the field of emerging engineering technologies.

The objectives of **SJET** are:

1. To bring new engineering ideas, research and findings on a single platform.
2. To integrate interdisciplinary research for technological sustainable solution.
3. To provide scholarly platform to connect academia and industries for socio-economic development.

Research Themes

The research focused on but not limited to following core thematic areas:

Renewable Energy Sources and Storage:

- Solar energy system fabrication and construction of advanced fuel cell technology
- Designing and analyzing smart hydro and wind energy systems
- Developing systems for biomass and bio-fuels
- Energy management and storage
- Energy devices and materials
- Energy harvesting for wireless and body sensor networks
- Energy efficiency and policies
- Energy devices and materials

- Design control and management
- Energy management and Environmental issues
- Hybrid power system
- Distributed and co-generation systems
- Power market and power system economics

Electrical Machines and Adjustable Speed Drives:

- AC and DC machines and drives
- Sensor-less control
- Piezo and electrostatic actuators
- Machine design and equipment training
- Maintenance and fault diagnosis
- Bearing less driving technologies

Power Systems and Smart Grids:

- Power Quality Issues and solutions
- Micro grid systems and their Integration Problems

Publisher: **Sukkur IBA Journal of Emerging Technologies (SJET)**
Office of Research, Innovation & Commercialization – ORIC
Sukkur IBA University - Airport Road Sukkur-65200, Sindh Pakistan

Tel: (09271) 5644233 -37 Fax: (092 71) 5804425 Email: sjet@iba-suk.edu.pk URL: sjet.iba-suk.edu.pk

Power Electronics and its Application:

- Hard-switching and soft-switching static converters
- Multi-level and matrix converters
- Emerging topologies
- Simulation and control power converters
- Power factor correctors
- Active filters and total harmonics distortions analysis
- Optoelectronics and photonic devices
- Power semiconductors, passive components, and packaging technologies
- Switch-mode power supplies and automotive
- Applications of power electronics in home appliance

High Voltage Engineering and Insulation Technology:

- Micro-electromechanical system (MEMS)
- Power Integrated circuits (PIC)
- Power Engineering related Technologies
- Power system stability and control
- Power system transient modeling, simulation and analysis
- Electromagnetic transient programs (EMTP)
- HVDC and FACTS applications

Nanomaterials/Nanotechnology:

- Sensors and Actuators
- Electronic Thin Films
- Nanogenerators
- Nanomaterials

- Nanotechnology optoelectronic sensors
- magnetic sensors
- thermal sensors
- mechanical sensors

Communication and Signal Processing:

- Communication & signal processing
- Radio frequency systems, microwave and antenna design
- Analog and mixed signal circuits
- Filter designing
- Satellite communication, mobile communication
- Cognitive and software design radio
- Analog and Mixed Signal Circuits

Biomedical Electronics:

- Energy-efficient wireless body sensor networks
- Wireless power/energy transfer in ehealth applications
- Green and battery-friendly wireless medical networks
- Renewable energy and energy harvesting for wireless and body sensor networks
- Telemedicine and medical IoT
- Medical video transmission
- Energy management for medical health applications
- Role of 5G in medical health applications

Thermal and complex fluid dynamics:

- Active and passive techniques for fluid flow manipulation

Publisher: Sukkur IBA Journal of Emerging Technologies (SJET)

Office of Research, Innovation & Commercialization – ORIC

Sukkur IBA University - Airport Road Sukkur-65200, Sindh Pakistan

Tel: (09271) 5644233 -37 Fax: (092 71) 5804425 Email: sjet@iba-suk.edu.pk URL: sjet.iba-suk.edu.pk

- Fluid flow process for industrial equipment's
- Modeling of working fluids
- Experimental fluid dynamics
- Multifunctional heat exchangers/chemical reactors
- Energy efficient combustion
- Environmental fluid flows
- Thick and thin films
- Optical glass fibers
- Amorphous
- Polycrystalline monocrystalline silicon, nanomaterials
- Synthesis of nanomaterials, composite materials
- Functional material
- Electronic thin films and integrated devices
- Engineering materials
- Solid and structural mechanics

Materials and their processing

- Piezoelectric materials
- Polymers, metal oxides
- III, V and II, VI semiconductors

Patron's Message

Sukkur IBA University has been imparting education with its core values merit, quality and excellence since its inception. Sukkur IBA University has achieved numerous milestones in a very short span of time that hardly any other university has achieved in the history of Pakistan. The institute continuously being ranked as one of the best Institute in Pakistan by Higher Education Commission (HEC). The distinct service of Sukkur IBA University is to serve rural areas of Sindh and also underprivileged areas of other provinces of Pakistan. Sukkur IBA University is committed to serve targeted youth of Pakistan who is suffering from poverty and deprived of equal opportunity to seek quality education. Sukkur IBA University is successfully undertaking its mission and objectives that lead Pakistan towards socio-economic prosperity.

In continuation of endeavors to touch new horizon in the field of Engineering and Emerging Technologies, Sukkur IBA University publishes an international referred journal. Sukkur IBA University believes that research is an integral part of modern learnings ad development. **Sukkur IBA Journal of Emerging Technologies (SJET)** is the modest effort to contribute and promote the research environment within the university and Pakistan as a whole. SJET is a peer-reviewed and multidisciplinary research journal to publish findings and results of the latest and innovative research in the fields. Following the tradition of Sukkur IBA University, SJET is also aimed at achieving international recognition and high impact research publication in the near future.

Prof. Nisar Ahmed Siddiqui
Sitara-e-Imtiaz
Vice Chancellor
Sukkur IBA University
Patron SJET

Publisher: **Sukkur IBA Journal of Emerging Technologies (SJET)**

Office of Research, Innovation & Commercialization – ORIC

Sukkur IBA University - Airport Road Sukkur-65200, Sindh Pakistan

Tel: (09271) 5644233 -37 Fax: (092 71) 5804425 Email: sjet@iba-suk.edu.pk URL: sjet.iba-suk.edu.pk

Editorial

Dear Readers,

It is immense pleasure to present you the Third issue of Sukkur IBA Journal of Emerging Technologies (SJET). Sukkur IBA University firmly believes in research environment and has provided a platform for the intellectuals and researchers to share knowledge and new findings on emerging trends in various research areas to solve the difficult technical problems related to the technological advancements in response to the demands of the times. The SJET provided interdisciplinary platform to researchers' community to collaborate, co-innovate and instigate efforts to break the technological barriers. This journal provides the opportunity to gain and present authentic and insightful scientific & technological information on the latest advances in the field of emerging technologies.

The SJET provides invaluable source of information and enables the interested researchers to access the original information they are seeking. The manuscripts submitted in SJET have been followed by double-blind peer-review process, which addresses key issues in the field of emerging engineering technologies. The SJET has endorsed highly standards which are prerequisite for publishing high quality research work. This journal manifests into eco-system for the academician and engineers work together in the pursuit of excellence & innovation, that is why the editorial board of SJET is comprises of academic and industrial researchers from various advanced countries. The journal has adopted Open access policy without charging any publication fees that will certainly increase the readership by providing free access to a wider audience.

On behalf of the SJET, I welcome the submissions for upcoming issue (Volume-2, issue-2, July–December, 2019) and looking forward to receive your valuable feedback.

I hope this journal will make a difference in our perspective and choice of research.

Sincerely,

Dr. Saeed Ahmed Khan

Chief Editor

SJET

Publisher: **Sukkur IBA Journal of Emerging Technologies (SJET)**

Office of Research, Innovation & Commercialization – ORIC

Sukkur IBA University - Airport Road Sukkur-65200, Sindh Pakistan

Tel: (09271) 5644233 -37 Fax: (092 71) 5804425 Email: sjet@iba-suk.edu.pk URL: sjet.iba-suk.edu.pk

Patron

Prof. Nisar Ahmed Siddique

Chief Editor

Dr. Saeed Ahmed Khan

Associate Editors

Dr. M Asim Samejo, Dr. Fareed Hussain Mangi, Dr. Arsalan

Managing editor

Dr. Yameen Sandhu, Dr. Syed Sabir Hussain Shah, Dr. Safeer Hyder Laghari

Editorial Board

Prof. Dr. B.S Chowdhry

Mehran University of Engineering & Technology,
Jamshoro

Prof. Dr. Mukhatiar Ahmed Unar

Mehran University of Engineering & Technology, Khairpur

Prof. Dr. Yuan Lin

University of Electronic Science and Technology of China

Prof. Dr. Jun Lin

School of Renewable Energy, North China Electric Power
University Beijing, China

Prof. Meicheng Li

School of Renewable Energy, North China Electric Power
University Beijing, China

Prof. Dr. Evaristo Musonda

School of Engineering, University of Zambia, Zambia

Dr. Sandeep Pirbhulal

Western Sydney University, Australia

Dr. Mehmet Yuceer

University of Leeds, UK

Dr. Sajid Ahmed

Information Technology University Lahore

Prof. Dr. Anderi Gurtov

Linkoping University Sweden

Prof. Dr. Qari Muhammad Khalid Waheed

University of Engineering & Technology, Peshawar

Prof. Dr. Florin Popentiu

University of Bucharest, Romania

Prof. Dr. Samir Muzaffar Iqbal

University of Texas Rio Grande Valley, USA

Dr. Huy-Dung Han

Department of Electronics and Computer Engineering,
Hanoi University of Science and Technology, Vietnam

Prof. Dr. Madad Ali Shah

BBS University of Technology and Skill Development,
Khairpur Mir's

Prof. Dr. M. Shahid Shaikh

Habib University, Karachi

Prof. Dr. Qamar ul Islam

Institute of Space Technology, Islamabad

Prof. Dr. Muhammad Ali Memon

Department of Electrical Engineering, NEDUET, Karachi

Dr. Abdul Rahman Abbasi

Karachi Institute of Power Engineering

Engr. Zahid Hussain Khand

Sukkur IBA University

Dr. Muhammad Asim Samejo

Sukkur IBA University

Dr. Faheem Akhtar

Sukkur IBA University

Dr. Abdul Qadir Rahimoon

Sukkur IBA University

Dr. Ali Hassan Sodhro

Sukkur IBA University

Language Editors

Prof. Ghulam Hussain Manganhar, Dr. Hassan Ali Shah
Sukkur IBA University, Pakistan

Project and Production Management

Mr. Hassan Abbas, Ms. Suman Najam Shaikh, Ms. Rakhi Batra

Publisher: **Sukkur IBA Journal of Emerging Technologies (SJET)**

Office of Research, Innovation & Commercialization – ORIC

Sukkur IBA University - Airport Road Sukkur-65200, Sindh Pakistan

Tel: (09271) 5644233 -37 Fax: (092 71) 5804425 Email: sjet@iba-suk.edu.pk URL: sjet.iba-suk.edu.pk

Contents

Investigation of LSB based Image Steganographic Techniques in Spatial Domain for Secure Communication (1-12)

Shahid Rahman, Fahad Masood, Wajid Ullah Khan, Abdus Salam, Syed Irfan Ullah

IoT Based Home Automation (13-19)

Abu Bakar Siddique Kamboh, Sanaullah Memon

Reactive Power Compensation using Matrix Converter: Indirect Space Vector Pulse Width Modulation Technique (20-26)

Muhammad Ishaq, Muhammad Hammad Afzal, Mukhtar Ali, Muhammad Waqar

Review on SCR catalysts by focusing impacts of sulfur on SCR Performance (27-44)

Ghazanfar Mehdi, Song Zhou, Yuanqing Zhu, Zubair Ali Shah, Kishore Chand, Raza Waleed, Asif Raza, Sanaullah

Stabilization of Non-holonomic 03 DOF Hovercraft using Robust RST Control Design (45-50)

Ghulam E Mustafa Abro, Bazgha Jabeen ,Abdul Manan

Effect of Tempering Temperature on the Properties of Martensitic Stainless Steel AISI-420 (51-56)

Iftikhar A. Channa, Aqeel Ahmed Shah, Shahid Hussain Abro, M. Ali Siddiqui, M. Mujahid, Ali Dad Chandio

Investigation of LSB based Image Steganographic Techniques in Spatial Domain for Secure Communication

Shahid Rahman¹, Fahad Masood¹, Wajid Ullah Khan¹, Abdus Salam¹, Syed Irfan Ullah¹

Abstract:

Confidentiality, integrity and authenticity for secure data are required for all the conveying bodies. Distinctive methodologies are utilized to adopt the security issues like digital certificate, digital signature and cryptography. These techniques alone cannot be traded off. Steganography is one of the answers to the security as it hides the secret information. Steganography has the importance in view of its exponential advancement and riddle data of possible PC customers over the web. It can likewise be depicted as the examination of indistinct information that usually manages the methodologies for concealing the closeness of the passed-on message. Mostly part of data covering is refined in correspondence to image, content, voice or sight and sound substance for copyright, military correspondence, confirmation and various diverse purposes. In this paper Least Significant Bit (LSB) technique for image steganography has been observed under various cases. Results for different scenarios have been looked at and the condition of the science assessment and examination of various accessible strategies for steganography have been given. The principles pursued are equivalent to give into the writing. Normal models and procedures drawn from the literature are utilized to obtain the results. This survey concludes with recommendations and supporters for the caries-oriented mechanism.

Keywords: *Steganography, Data concealing, Cover writing*

1. Introduction

Steganography is derived from two Greek words, "Steganos" means 'covered/protected' and "graphic" representing "writing". So Steganography infers covered writing. It is one of a kind branches of "information stowing away or hiding". It is characterized as "The way towards composing secret message with the end goal that the nearness of the message is just known to the sender and receiver"[1]. It is the workmanship and study of undetectable communication and a push to cover the presence of the embedding data. Cover steganography is the art of conveying information that can't be distinguished or detected [2]. Steganography not only changes the course of action of the mysterious

message, but also covers it inside a cover-dissent or question. Resulting to conceal strategy cover test and stego-Image (passing on secured data contradict) is indistinguishable. In this manner, steganography (concealing data) and cryptography (anchoring data) are absolutely astonishing from one another. By virtue of subtlety or shrouded factors it is hard to recuperate the data without knowing the framework in steganography. Systems for steganography insinuated as Steganalysis are the same as cryptanalysis [3].

A. Digital medium for steganography

There are five types of Steganography techniques used for embedding secret messages depending upon a cover protest or object.

¹ Department of Computing Abasyn University Peshawar KPK, Pakistan
Corresponding Author: rahmanshahid@gmail.com

i) **Image Steganography:** A steganography type, in which image is used as a cover object. In this framework, pixel energy of the cover image is utilized to cover information. Images are thought to be the best cover objects for disguising information since it contains a generous measure of respective bits [4].

ii) **Network Steganography:** In network Steganography, network protocols are used as cover object such as TCP, IP, UDP and ICMP and so on. Data is covered up in a few fields of the header of TCP/IP packet that are open or never utilized [5].

iii) **Audio Steganography:** In this type audio is utilized as a cover object for data embedding. It has turned out to be an extremely critical medium because of voice over IP (VOIP) factor. It uses some digital plans like as Waveform Audio file format (WAVE), Audio Video Interleave (AVI), Moving Picture Experts Group (MPED), Musical Instrument Digital Interface (MIDI) etc. [6].

iv) **Video Steganography:** In video Steganography, collection of an image (video) is utilized as a cover object for concealing data. This strategy is able to shroud any type of records or data into computerized video design. Discrete cosine transforms usually modify values 8.667 - 9. Shrouded information for every image in video is utilized which is not recognizable by the HVS. The formats utilized by video steganography are Mp4, MPEG, H.264, and AVI and so on [7, 8].

vi) **Text Steganography:** In text Steganography text is utilized as a cover object. In this strategy mystery message is covered up in the nth letter of each cover text. Text steganography is thought to be the most difficult type of steganography because of the absence of excess in text when contrasted with different kinds of steganography. However, it requires less memory and is used for straightforward information [8]. Fig.1 shows the digital mediums for steganography.

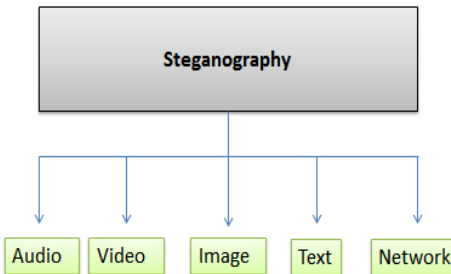


Fig.1. Digital Medium of Steganography

B. Structure of Steganography

Steganography has three main parts.

i) **The Cover or Carrier:** It can be an image or painting, a digital image (tiff, jpg, bmp, png), an mp3 (audio files), a text file, a video file or TCP/IP packet as well. It is the object that will carry the hidden message.

ii) **The Message:** It can be a simple text or content, a secret image, an audio or video which will be transmitted securely.

iii) **The Key:** It can be a password, pattern, a black-light or a pseudo random number known to both sender and receiver. It is used at the time of embedding and extraction of secret information. It provides more protection against third parties/hackers.

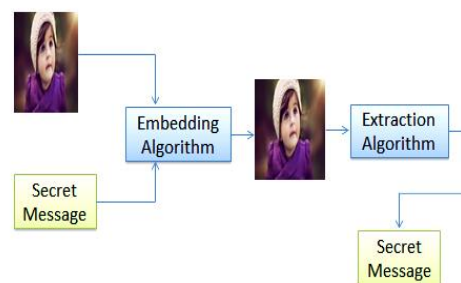


Fig.2. Image Steganography [1]

Fig.2 shows a fundamental plan of image steganography. Secret image is hidden within the image in such a manner that the intended

user is prevented to detect the hidden message. Stego-image is formed through an embedding algorithm. The stego- images when formed have a mirror distortion of the image which is negligible for the naked eye. The hidden message can be an extracted algorithm from the stego-object.

C. Categorizations of image steganography

Image steganography is classified in different types on the basis of measuring algorithm which is shown in table-1[10].

i) **Perceptual Transparency:** Once procedure is concealed into a carrier object, detectable quality will be debased into embedded image as equate with the original-object.

ii) **High Payload or Capacity:** In cover object extreme mass of information can be inserted.

iii) **Robustness:** Information should remain in place after covering, if embedded -image is changed, For example, editing, filtering, scaling and expansion of clamor (noise).

iv) **Temper protection:** It is a problematic issue to change the secret message after it has been secured into embedded object.

v) **Calculation Complexity:** How much costly it is computationally to embed and extract a covered message?

Table I: MEASURING ALGORITHM

Measures	Advantages	Disadvantages
Perceptual Transparency(HVS)	High	Low
High Capacity (Pay Load)	High	Low
Calculation Complexity	Low	High
Robustness (Security)	High	Low
Temper protection	High	Low

Table 1 shows the measuring algorithms for steganography, which is the basic criteria of steganography which will be analyzed through different existing methods in spatial domain based on these measuring algorithms which is shown in Table V.

D. Techniques of Image steganography

Image or image steganography plans can be confined into following area:

i) **Methods of Spatial Domain:** In spatial steganography distinctive executions are available. LSB based steganography is one of the smallest complex techniques that covers an inside secret message in the LSB's of pixel without showing different distinguishable damages or twisting. Changes in the estimation of the LSB are refined or impalpable for HVS. Some standard approaches in spatial domains are given below:

- EBE (Edges based embedding method)
- LSB (Least significant bit)
- RPE (Random pixel embedding method)
- Gray level modification and Multi level Encryption (MLE)
- Hidden data pixel mapping method
- Connectivity method or labelling
- Cyclic steganography randomization methods
- Pixel value differencing (PVD)
- Method of Pixel intensity
- Method of content or texture
- Shifting methods of Histogram

There are some common focal points and weakness of a spatial area based on LSB methods:

Focal points:

- Lesser shot for debasement of the cover object.
- In the image extreme size of data or information can be embedded.

Weaknesses:

- Less energy, with manipulation of image concealed information can be lost.
- Concealed data can be effectively crushed by open assaults if there is no robustness.

ii) **Transform domain:** In this technique we initially change the image from spatial space in recurrence area, conceal the mystery message and change it to the spatial domain. To conceal data utilizing these systems,

distinctive calculations and changes are connected with images which increment its many-sided quality. This strategy is thought to be considerably more grounded than spatial domain procedures. This method shroud data in those territories of the image that are less powerless by image pressure, trimming, and cropping. This system less inclined to measurable assaults and image corruption is additionally kept at least as we change proficient in the change space, they have also brought down the payload and not are against editing, turn, interpretation and commotion [11]. Some Transform domain methods are:

Coefficient bits embedding

- Reversible method or lossless
- Discrete Fourier Transform (DFT)
- Discrete Wavelet Transform (DWT)
- Discrete Cosine Transform (DCT)

iii) Misrepresentations or Distortion Techniques:

In this framework we require information of the chief cover picture with the confining strategy. Here the decoder capacity check between the primary cover picture and the wasted cover picture with a specific extreme target to re-establish the mystery message. The encoder adds a social occasion of advancement to the cover challenge. Thus, data is explained as being secured by flag twisting [12]. Using this structure, a stego dissent or question is made by applying a course of action for adjustment of the cover picture. This movement of modification is used to rewrite the problem message required to transmit [13]. The message is encoded in pseudo-haphazardly picked pixels. The stego-picture is fascinating in association with the cover picture at the given message pixel, the message bit is a "1." normally it is "0". The encoder can change the "1" respect pixels in such a course to the point that the honest properties of the picture are not influenced. Regardless the need for sending the cover picture restrains the upside of this framework. In any steganographic structure, the cover picture to never be utilized more than once. On the off chance that an aggressor changes the stego-picture by altering, scaling or turning, the beneficiary cannot recollect it. From time to time, if the message is encoded with spoil reviewing the data, the change can even be traded and the fundamental message can be recovered [14].

iv) **Filtering and Masking:** This method conceals data by denoting an image similarly as paper watermark. This strategy embeds the data in the huger regions than simply concealing it into the noise level. The concealed message is more important to cover picture. They are more joined into the picture when watermarking methods can be associated without the fear of picture damage in light of pressure.

Some focal points and weaknesses of filtering and masking techniques:

Focal point:

- Significantly the said technique is much powerful as compared to least significant bit. Data is covered up into unmistakable slices of the image or picture.

Weaknesses:

- Strategies can be associated just excessively dim or dark scale pictures and restrict it to 24 bits.

2. Analysis

Steganography is an upcoming research area that uses images, videos, and network protocols, and audio for information concealment. From the last time in the spatial domain, several approaches for digital steganography have been proposed. These approaches are based on LSB substitution, edge based embedded, and pixel indicator based embedded.

Every approach has its relating advantages and disadvantages. Some methods have high payload limits and great softness were blurriness depend on the chosen cover for covert or unknown information, concealing (Spatial domain) but more vulnerable against assaults (Noise tossing, rotation, revolution, resizing and so forth) while other schemes are strong against factual or statistical assaults, so far, they have brought down payload boundary. This implies that is reliably an exchange off between the three mechanisms (Payload, Imperceptibility& Robustness).

We will summarize different methods with their related advantages and disadvantages based on image steganography, which is discussed one by one below.

Hanling et al. proposed a new pixel esteem (value) differencing procedure; for data embedding near the goal pixel it used the three pixels. It utilizes essential k-bit LSB technique for mystery information implanting with high refinement regard where the number of k-bit is assessed by pretty much three pixels. It basically uses a perfect pixel adjustment method on target pixels to hold better visual quality and high breaking point. Histogram of stego-picture and cover-picture is generally same in the great position of the procedure, however dataset for tests are closed to nothing [15].

Channalli et al. proposed LSB based picture covering approach. Conventional outline bits (stego-key) are utilized to cover information. The minimum noteworthy piece of the pixel is adjusted relying on the (stego-key) layout bits and the secret message bits. Representation bits are composite of MxN measure lines and regions (of a piece) and with erratic key esteem. Whenever fulfilled it change the second LSB bits of cover picture generally continues as already. Every illustration bit is facilitated with the message bit in covering the system. This method centers to achieve security of masked message in the stego-picture using a run of the mill case key. The major disadvantage in the proposed procedure his a low covered farthest point since single secured bit requires a bit of (MxN) pixel [16].

Jung, K. H et al. proposed a strategy for Multi-Pixel Differencing (MPD) for data implanting, It process aggregate of refinement estimation of four pixels square and uses extra two pixels to scale smoothness of each pixel. It is utilized for little refinement esteem. For high complexity esteem it uses a multi pixel differencing system for data covering. So exploratory dataset is too much obliged, but quality is its straightforwardness of figuring [17].

Yang, et al. proposed a data covering methodology to cover the data using LSB where it finds the darkness locale of the picture. Using 8 pixels organize plans for concealing data bits; it changes over it to two-fold picture and denotes each dissent. The strategy requires high tally to discover

diminish region. Its openness and has no endeavoured to high surface sort of picture. Thoroughly, endless supply of image which covers its limits. [18]

Mahdi et al. proposed another picture steganography strategy, with assertion of emotional pixel of the required picture region and in light of LSB substitution. The mystery key is incorporated by LSB pixels this technique is centred to upgrade. A Mystery message must be concealed if it creates irregular numbers and picks the region by combining. It is not yet considered a perceptual straightforwardness but the nature of the technique is its security of hiding messages in stego-image. [19].

Babita et al. proposed a new image steganography method, to embed data. It uses 4 LSB of each RGB channel. It applies focuses sifting to upgrade the possibility of the stego picture and encodes the refinement of cover and stego picture as key information. To isolate the covered data in separating stage the stego-picture is added with key data. It also needs to supervise stego-key which it fabricates the multifaceted nature of applying filters. The major demerit of the proposed scheme is covering limit of high secret data. [20].

Bailey et al. proposed stego shading cycle (SCC) strategy for shading images that conceals information in various channels of the cover image in a cyclic way. The primary mystery bit is covered up in pixel1's red channel, the second mystery bit is covered up in the green channel of pixel2 and the third mystery bit is covered up in the blue channel of pixel3. The significant confinement in SCC technique is that the mystery data is installed in cover image pixels in a settled cyclic and orderly way. So, aggressors can without much of a stretch find this strategy if mystery data from a couple of pixels is effectively separated [21].

Gutub et al. proposed a high payload pixel pointer method (PIT) what one channel is utilized as a marker and the other two channels are information channels. The proposed strategy shrouded the puzzle information in either of the information which

directs in a predefined cyclic way. The provisional outcomes demonstrate the incredible limit and better delicate quality of the arranged calculation and furthermore dodge the key trade overhead. The major feeble purpose of this technique is that the payload limit is absolutely subject to have pictures and marker bits which can result in low payload. Similarly, this method hides fixed numbers of bits in each pixel which can be brought more changes in the cover image if we embed a greater number of secret bits in each pixel. The major limitation in the proposed method is that the secret information can be extracted easily if an attacker finds out the algorithm being used for message hiding because secret data is in plain text form not encrypted. Moreover, these methods result in stego images of low quality which can be detected using HVS [22].

Karim et.al presented a new approach to enhance the security of the existing LSB substitution method by adding one extra barrier of the secret key. In the said method, secret key and red channel are used as an indicator while green and blue channels are data channels. Basis of covered key bits and red channel LSBs the secret data bits are embedded either in green channel or in the blue channel. If either the bit of the red channel LSB or the secret key bit is 1, then the LSB of green channel is replaced with secret message bits otherwise LSB of blue channel is replaced by secret bit. Although this approach possesses the same payload as LSB based approaches, it increases security by making the use of a secret key. An intruder cannot easily extract the secret information without the correct secret key [23].

Muhammad et.al presents an ensured strategy for shading picture steganography using gray-level modification and multilevel encryption. The security of information between two social gatherings is noteworthy issue in this front-line area. To adjust these issues proposed plot is a viable procedure for RGB pictures in light of diminishing or dim dimension change gray level modification (GLM) and staggered encryption (MLE). The mystery key and secret information are encoded utilizing MLE calculation before mapping it to the dark levels of the cover

image. At this point, a transposition work is connected on cover image preceding information stowing away. The use of the transpose mystery key, MLE, and GLM includes four unique levels of security to the proposed calculation making it extremely troublesome for a vindictive client to extricate the first secret data. However, the proposed scheme provides a robust, efficient and time saving way to hide secret information inside the cover image. The main advantages of the proposed scheme improve quality of stego images, high imperceptibility, cost-effectiveness, and enhanced robustness. Moreover, the utilization of MLE and image transposition adds multiple security levels to the said technique. The major shortcoming of this method is its vulnerability to different attacks (cropping, scaling and noise attacks) which exist in all spatial domain techniques including the existing five schemes. Since the spatial domain is used in the proposed approach, the hidden data cannot be fully recovered if the image is compressed, scaled or attacked with noises [24].

F. A Jassim et al proposed a protected strategy whose key thought depends on the way that adjoining pixels in pictures are firmly connected with one another. In FMM plot, the picture is isolated into various obstructs, every one of which contains $k \times k$ pixels where k demonstrates the window measure and every pixel speaks to a number in the range 0-255 distinct by 5 for 8-bit pictures. The proposed ST-FMM strategy is better in power and accomplishes great nature of stego pictures. In any case, there is an exchange off between the payload and window size with the end goal that expands the window estimate diminishes the payload and the other way around [25].

Wang, et al proposed a superb steganographic technique dependent on pixel value differencing (PVD) and modulus work, which is more secure against the different identification assault and performs superior to anything the PVD conspire. This plan expands the pinnacle motion (PSNR) qualities to 44.15 dB while disguised 51,219 bytes. It abuses the rest of the two continuous pixels to record the data of the inserted information. It accomplishes greater adaptability, fit for

determining the ideal rest of the two pixels in any event mutilation. This strategy expands the PSNR (up to 8.9%) more than the straightforward PVD technique. To keep up the distinction in a similar range when inserting process, this technique utilizes rearranging system to change the notice of the pixel combine [26].

Joo, et al. exhibited an improvement on [32] technique by installing distinctive measures of mystery information depending on pixel-match intricacy. The test in this strategy demonstrates that the distinction histogram had a shape nearer to the cover-picture which was difficult to be identified by histogram examination. Despite the fact that this technique enhanced the issue of the shape in the distinction histograms. The inserting limit isn't higher than Wang et al strategy, which is differing for the odd and even implanting zones [27].

Chen et al presented a PVD strategy utilizing pixel pair matching (PPM). In this strategy, the cover-picture is apportioned into 2×2 inserting cells for installing by arbitrary implanting plans. To expand the arbitrary inserting trademark, two reference tables are made. This irregular system raises the security of the implanted information from discovery and different steganalysis assaults. The real commitments of this methodology are: (1) PPM was used subsequently a bigger number of information disguised than unique PVD, (2) Effectively diminishing the tumbling off-limit issue of controlling just on Pivot Embedding Unit (PEU). (3) The mystery information was covered which was dependent on two reference tables which raised the irregular trademark and the visual quality. (4) This strategy is harder to be recognized for its distinction histogram. It shows that the estimations of the stego-picture are near the estimations of the cover-picture. Chen plot altogether had higher limit and picture quality [28].

Al Dhamari et al proposed another square based steganographic calculation utilizing PVD and modulus work procedures, to be specific, MF-PVD. To assess the execution of MF-PVD calculation, they contrast it and six relevant conditions of-workmanship calculations, as an obvious truth, the proposed

MF-PVD calculation is exceptional to these reference techniques in two fundamental highlights, the inserting limit and the security. Actually, the security of calculation is high because of producing numerous stages and existing the separate extend table. The calculation's system can be stretched out to the RGB shading pictures for enhancing the ability of inserting. In addition, it may be a decent expansion to build up a methodology that considers the half breed area. So there are tentative arrangements to create modulus work based plans for other media, for example, sounds and video [29].

Khan et al proposed a novel picture steganographic procedure (M-LSB-SM) for shading pictures with better indistinctness and security. A normal PSNR of 47.93 dB is registered more than one hundred and fifty pictures. The mystery data are separated into four sub-squares and is gone through MLEA, which makes the assault on this calculation dreadful and therefore, deceives the procedure of steganalysis. This is the reason that their proposed plan is equipped for producing stego pictures of an adequate quality that satisfies the ideal requests of current security frameworks and clients. The calculation is straightforward, simple to execute and a decent blend of subtlety and security and therefore is more possible to be embraced by steganographic applications. Still extra upgrades are feasible broadening MLE calculation and payload capacity.

Table II shows the analysis of different image steganographic techniques in spatial domain based on PSNR in the range of 50-65.

Table III shows the analysis of different image steganographic techniques in spatial domain based on PSNR in the range of 45-50
Table IV shows the analysis of different image steganographic techniques in spatial domain based on PSNR in the range of 38-45.

Table II: Analysis of Different Image Steganographic Techniques in Spatial Domain Based on PSNR in the Range of 50-65

S.NO	Existing Methods	PSNR Values
1	Khan et al method 2[36]	63.0034
2	Khan et al method 1[24]	58.7344
3	Karim's Method[23]	52.2172
4	Classic LSB Method[7]	52.2416
5	SCC Method[27]	52.2023
6	Channali et al [16]	51.9764

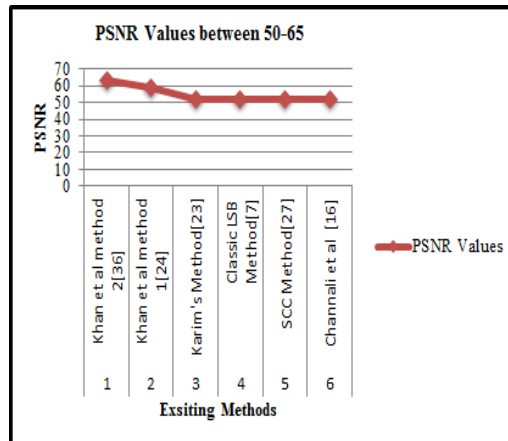


Fig.3. PSNR values of Exsiting methods Between 50-65

Figure 3 shows the analysis of different image steganographic techniques in spatial domain based on PSNR in the range of 50-65. It seems that khan et al method [36] having PSNR value 63.0034 which dominate over all other methods, that show the visual quality of the image.

Table III.: Analysis of Different Image Steganographic Techniques in Spatial Domain Based on PSNR in the Range of 45-50

S.NO	Existing Methods	PSNR Values
1	Hangling et al [15]	49.5545
2	Wang et al [32]	49.2565
3	PIT [11]	48.5249
4	Mehdi et al [19]	48.2454
5	Gutub et al [22]	47.4536
6	Jung K H et al [17]	45.5677

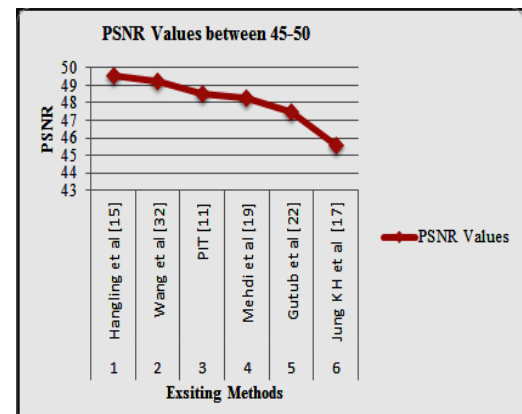


Fig.4. PSNR values of Exsiting methods Between 45-50

Figure 4 shows the analysis of different image steganographic techniques in spatial domain based on PSNR in the range of 45-50. It seems that Hangling et al method [15] having PSNR value 49.5545 which dominate over all other methods, that show the visual quality of the image.

Table IV: Analysis of Different Image Steganographic Techniques in Spatial Domain Based on PSNR in the Range of 38-45

S.NO	Existing Methods	PSNR Values
1	F A jassm et al [25]	44.3455
2	Baily et al [21]	43.3425
3	Joo et al [33]	42.5352
4	Yang et al [18]	42.4553
5	FMM[26]	41.294 4
6	Al Dhamari et al [35]	39.5676

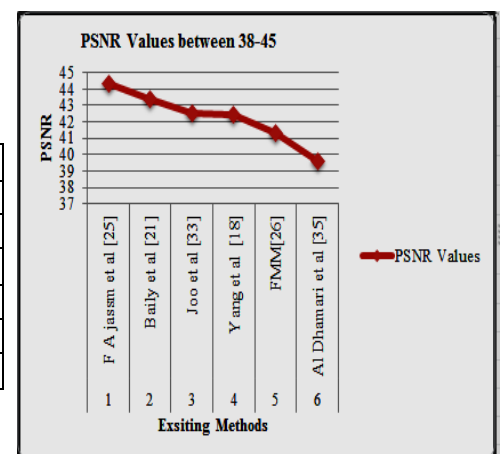


Fig.5. PSNR values of Exsiting methods Between 38-45

Figure 5 shows the analysis of different image steganographic techniques in spatial domain based on PSNR in the range of 38-45. It seems that F A jassm et al method [25] having PSNR value 44.3455 which dominates over all other methods, that show the visual quality of the image.

Table.V shows critical analysis up to eighteen methods with their advantages and disadvantages and also analyzed based on measuring algorithm (Capacity, Robustness, Perception, Temp protection, computation) which is the basic criteria of steganography, which is also shown in Table I.

3. Conclusion and Future Work

Specialists have introduced different plans to adapt web security issues. In this specific situation, both steganography and cryptography can be utilized successfully. However, real restriction in the current steganographic techniques is the low-quality yield stego images, which subsequently brings about the absence of security.

This paper provides an illustration of a number of steganographic methods; its significant kinds and arrangement of steganography in the recent couple of years have been proposed. We have dissected various proposed systems. It is demonstrated the visual nature of the image is corrupted when shrouded information expanded up as far as possible utilizing LSB based strategies. Analysis of the truthful properties of commotion or visually investigation strategies can be broken or demonstrates significant adjustment of image.

In this study, distinctive steganographic articles were contemplated and were ordered into various methods. The same numbers of new application zones are recognized like web managing an account, portable correspondence security, cloud security and so on. The understanding into the steganographic standards will certainly control us to recognize new zones and to enhance its applications in the effectively existing application regions also.

ACKNOWLEDGEMENT

The authors wish to thank every one of the supporters for their basic and specialized review of the proposed work and their important help and direction. The authors also gratefully acknowledge the helpful comments and suggestions of the reviewers.

Table V: Investigation of Different Image Steganography Techniques in Spatial Domain

SNo	Domain	Techniques	Advantages	Disadvantages	Analysis based on				
					Capacity	Robustness	Perception	Temp protection.	computation
1	Spatial[15]	PVD with Adaptive LSB	Histogram of both original and stego image is always same	for experimental results Data sets is too small	Yes	Yes	No	No	No
2	Spatial[16]	Pattern bits combinations along with (Stego-Key) using LSB	Hidden Data	Hidden Capacity is Low	No	No	No	No	No
3	Spatial[17]	MPD with LSB	Same as PVD but on some level is valuable from common PVD methods	Limited data sets, and Threshold, both sides Stego key require	Yes	Yes	No	No	No
4	Spatial[18]	Dark area of image with LSB substitution	Helpful for smooth district with strong limit of object based dataset	High calculation required and not tried on high surface zones	No	Yes	No	No	No
5	Spatial[19]	LSB substitution with Random pixel selection	Safety of hidden message in Stego-image	Implanting without thinking about Graphic Quality in Arbitrary pixel determination	No	No	No	No	No
6	Spatial[20]	LSB substitution with Median Filtering	High hidden capacity	Computationally confusing (sifting) in Stego-key essential	Yes	No	No	No	No
7	Spatial[21]	Stego Colour Cycle	Hiding data different channels	Embedding is a fixed cyclic and systematic way, easily can extracted if a few bit extracted	Yes	No	Yes	No	No
8	Spatial[22]	PIT	High hidden data better imperceptibility	shipment limit is absolutely reliant on host picture and pointer bits	Yes	Yes	Yes	No	No
9	Spatial[23]	LSB substitution replacement method	High payload , better imperceptibility by adding one extra barrier of secret key	Increasing security depending on secret key can easily extracted without correct key	Yes	Yes	Yes	No	Yes
10	Spatial[24]	GL- Modification and MLE	high imperceptibility, times Saving and robustness	vulnerability to different attacks (cropping, scaling and noise)	No	Yes	Yes	Yes	Yes
11	Spatial[31]	hiding text in image using five modulus method	Achievement of robustness and good quality of stego images	If increasing the window size then will be decrease payload	Yes	No	Yes	No	No
12	Spatial[32]	pixel-esteem differencing and modulus work	High Capacity, and good Image quality	vulnerability to different attacks	Yes	No	Yes	No	No
13	Spatial[33]	protecting pixel-esteem differencing histogram with modulus work	Enhanced Security and perception transparency	Hidden data too low	No	Yes	Yes	No	Yes
14	Spatial[34]	histogram preserving using pixel pair matching	Higher limit and Better Quality	vulnerability to different attacks	Yes	No	Yes	No	Yes
15	Spatial[35]	modulus function and pixel-value differencing	Embedding capacity and the security	Perception and vulnerability to different attacks(Noise ,cropping)	Yes	Yes	No	No	Yes
16	Spatial[36]	MLE and achromatic component of an image	Security and good imperceptibility	visual quality, payload limit and vulnerability of statistical attacks	No	Yes	Yes	No	Yes
17	Spatial[38]	Data Mapping and LSB Substitution	Embedding capacity and visual quality	Temper protection and computation	Yes	Yes	Yes	No	No
18	Spatial [39]	logistic map and secret key	High security, payload, Visual quality	Vulnerabilities(noise, cropping) computation	Yes	No	Yes	Yes	No

REFERENCES

- [1] Anderson, R. J., & Petitcolas, F. A. (1998). On the limits of steganography. *IEEE Journal on selected areas in communications*, 16(4), 474-481.
- [2] I. Diop, S. Farss, K. Tall, P. Fall, M. Diouf, and A. Diop, "Adaptive Steganography scheme based on LDPC codes," in *Advanced Communication Technology (ICACT), 2014 16th International Conference on*, 2014, pp. 162-166.
- [3] Pfitzmann, B. (1996, May). Information hiding terminology-results of an informal plenary meeting and additional proposals. In *Proceedings of the First International Workshop on Information Hiding* (pp. 347-350). Springer-Verlag.
- [4] Johnson, N. F., & Jajodia, S. (1998). Exploring steganography: Seeing the unseen. *Computer*, 31(2).
- [5] Ker, A. D. (2005). Steganalysis of LSB matching in grayscale images. *IEEE signal processing letters*, 12(6), 441-444.
- [6] Kour, J., & Verma, D. (2014). Steganography Techniques-A Review Paper. *International Journal of Emerging Research in Management &Technology ISSN*, 2278-9359.
- [7] A. Sharp, Q. Qi, Y. Yang, D. Peng, and H. Sharif, "A video steganography attack using multi-dimensional Discrete Spring Transform," in *Signal and Image Processing Applications (ICSIPA), 2013 IEEE International Conference on*, 2013, pp. 182-186.
- [8] Hu, S. D. (2011, August). A novel video steganography based on non-uniform rectangular partition. In *The 14th IEEE International Conference on Computational Science and Engineering* (pp. 57-61). IEEE.
- [9] Johnson, N. F., & Jajodia, S. (1998). Exploring steganography: Seeing the unseen. *Computer*, 31(2)..
- [10] Lin, E. T., & Delp, E. J. (1999, April). A review of data hiding in digital images. In *PICS* (Vol. 299, pp. 274-278).
- [11] Johnson, N. F., & Katzenbeisser, S. (2000). A survey of steganographic techniques. In *Information hiding* (pp. 43-78).
- [12] Reddy, H. M., & Raja, K. B. (2009). High capacity and security steganography using discrete wavelet transform. *International Journal of Computer Science and Security (IJCSS)*, 3(6), 462.
- [13] Aos, A. Z., Naji, A. W., Hameed, S. A., Othman, F., & Zaidan, B. B. (2009, April). Approved Undetectable-Antivirus Steganography for Multimedia Information in PE-File. In *Computer Science and Information Technology-Spring Conference, 2009. IACSITSC'09. International Association of*(pp. 437-441). IEEE.
- [14] Kruus, P., Scace, C., Heyman, M., & Mundy, M. (2003). A survey of steganography techniques for image files. *Advanced Security Research Journal.[On line]*, 5(1), 41-52.
- [15] Hanling, Z., Guangzhi, G., & Caiqiong, X. (2009, May). Image steganography using pixel-value differencing. In *Electronic Commerce and Security, 2009. ISECS'09. Second International Symposium on* (Vol. 2, pp. 109-112). IEEE..
- [16] Channalli, S., & Jadhav, A. (2009). Steganography an art of hiding data. *arXiv preprint arXiv:0912.2319*.
- [17] Jung, K. H., Ha, K. J., & Yoo, K. Y. (2008, August). Image data hiding method based on multi-pixel differencing and LSB substitution methods. In *Convergence and Hybrid Information Technology, 2008. ICHIT'08. International Conference on* (pp. 355-358). IEEE.
- [18] Yang, C. H., Weng, C. Y., Wang, S. J., & Sun, H. M. (2008). Adaptive data hiding in edge areas of images with spatial LSB domain systems. *IEEE Transactions on Information Forensics and Security*, 3(3), 488-497..
- [19] Islam, A. U., Khalid, F., Shah, M., Khan, Z., Mahmood, T., Khan, A., ... & Naeem, M. (2016, August). An improved image steganography technique based on MSB using bit differencing. In *Innovative Computing Technology (INTECH), 2016 Sixth International Conference on* (pp. 265-269). IEEE.
- [20] Chen, W. J., Chang, C. C., & Le, T. H. N. (2010). High payload steganography mechanism using hybrid edge detector. *Expert Systems with applications*, 37(4), 3292-3301..
- [21] Motameni, H., Norouzi, M., Jahandar, M., & Hatami, A. (2007). Labeling method in Steganography. *World Academy of Science, Engineering and Technology*, 24, 349-354...
- [22] Viswanatham, V. M., & Manikonda, J. (2010). A novel technique for embedding data in spatial domain. *International Journal on Computer Science and Engineering, IJCSE*, 2(2010)....
- [23] Yang, H., Sun, X., & Sun, G. (2009). A high-capacity image data hiding scheme using adaptive LSB

- substitution. *Radioengineering*, 18(4), 509-516.
- [24] Parvez, M. T., & Gutub, A. A. A. (2008, December). RGB intensity based variable-bits image steganography. In *Asia-Pacific Services Computing Conference, 2008. APSCC'08. IEEE* (pp. 1322-1327). IEEE.
- [25] F. A. Jassim, "A novel steganography algorithm for hiding text in image using five modulus method," *arXiv preprint arXiv:1307.0642*, 2013. Article (CrossRef Link)
- [26] Wang, C. M., Wu, N. I., Tsai, C. S., & Hwang, M. S. (2008). A high quality steganographic method with pixel-value differencing and modulus function. *Journal of Systems and Software*, 81(1), 150-158..
- [27] Joo, J. C., Lee, H. Y., & Lee, H. K. (2010). Improved steganographic method preserving pixel-value differencing histogram with modulus function. *EURASIP Journal on Advances in Signal Processing*, 2010(1), 249826.
- [28] Chen, J. (2014). A PVD-based data hiding method with histogram preserving using pixel pair matching. *Signal Processing: Image Communication*, 29(3), 375-384.
- [29] Al-Dhamari, A. K., & Darabkh, K. A. (2017). Block-based steganographic algorithm using modulus function and pixel-value differencing. *Journal of Software Engineering and Applications*, 10(01), 56.
- [33] Muhammad, K., Ahmad, J., Farman, H., Jan, Z., Sajjad, M., & Baik, S. W. (2015). A Secure Method for Color Image Steganography using Gray-Level Modification and Multi-level Encryption. *TIIS*, 9(5), 1938-1962..
- [34] Zakaria, A., Hussain, M., Wahab, A., Idris, M., Abdullah, N., & Jung, K. H. (2018). High-Capacity Image Steganography with Minimum Modified Bits Based on Data Mapping and LSB Substitution. *Applied Sciences*, 8(11), 2199.
- [35] Majeed, A., Mat Kiah, M. L., Madhloom, H. T., Zaidan, B. B., & Zaidan, A. A. (2009). Novel approach for high secure and high rate data hidden in the image using image texture analysis. *International Journal of Engineering and Technology*, 1(2), 63-69..
- [36] Muhammad, K., Sajjad, M., Mehmood, I., Rho, S., & Baik, S. W. (2016). A novel magic LSB substitution method (M-LSB-SM) using multi-level encryption and achromatic component of an image.
- Multimedia Tools and Applications, 75(22), 14867-14893.
- [37] Solanki, R., Chuahan, M., & Desai, M. SURVEY OF IMAGE STEGANOGRAPHY TECHNIQUES..
- [38] Bandhyopadhyay, A., Dey, D., Pal, R. K., & Maji, A. K. (2018). An Indirect Addressing Image Steganographic Scheme Using 9×9 Sudoku Matrix. In *Proceedings of the International Conference on Computing and Communication Systems* (pp. 689-703). Springer, Singapore.
- [39] Ulker, M., & Arslan, B. (2018, March). A novel secure model: Image steganography with logistic map and secret key. In *Digital Forensic and Security (ISDFS), 2018 6th International Symposium on* (pp. 1-5). IEEE.
- [40] Liao, X., Yin, J., Guo, S., Li, X., & Sangaiah, A. K. (2018). Medical JPEG image steganography based on preserving inter-block dependencies. *Computers & Electrical Engineering*, 67, 320-329.

IoT Based Home Automation

Abu Bakar Siddique Kamboh¹, Sanaullah Memon²

Abstract:

IOT or the internet of things is an upcoming technology that allows us to control hardware devices through the internet. Here we propose to use the IOT in order to control home appliances, thus automating modern homes through the internet. The main purpose is to control any electric supply equipment load through the Internet network over cloud remotely on the basic principle of the Internet of things (IoT). In this proposed research work, the real-time scenario the electric load can be monitored as well as configured through web-based applications. The data sent from any password protected device through a webpage. A Wi-Fi adapter is configured with the wireless modem to access the internet. The received internet commands are put into the Wi-Fi module. IoT offers a wide scope of new advancements for observing and controlling, of clever structures and keen homes, by improving security to lessen vitality and support costs. With the home computerization control framework, we make our home gadgets shrewd. Savvy, as in, the gadgets can be checked or perform a task as per the client's guidelines. For instance, an entryway lock framework where on the off chance that anybody obscures individual attempts to go into the house without approval, at that point the entryway, lock will initiate an alert connected to the entryway and in this we can say our house is sufficiently brilliant to give us security.

Keywords: *Internet of Things (IoT), Cloud, IPv4, Machine to machine (M2M), OSPF, DHCP.*

1. Introduction

The Internet of Things (IoT) is a name that has been broadly perceived since the late 1990s. The IoT is an arrangement of physical things that open through the Internet. The term "Internet of Things" (IoT) was first used in 1999 by British technology pioneer Kevin Ashton to describe a system in which objects in the physical world could be connected to the Internet by sensors. The IoT is highlighted as one of the most important future technology and is getting vast attention from all over the world [1].

Homes of the 21st century will turn out to be increasingly more self-controlled and robotized because of the comfort it gives, particularly when utilized in a private home. A home robotization framework that enables clients to control electric apparatuses of a differing kind.

The primary registering gadgets (PCs) were monsters, a room-sized mechanical assembly that took groups of individuals to configuration, handle and keep up. Nowadays, they are exponentially quicker and just a variety of the extent of their ancestors. A gadget is electronic appliance that performs computations dependent on these principle segments: a processor, storage, and Input & output unit.

The smart thermostat runs the program by using a processor, store the programs of temperature parameters in storage and other data, and an I/O (screen, show, sound cautions, and so on).

2. Background

IoT aims is to form a network between Home appliance objects and the sensors that can save, examine, communicate and barter data together on the internet. This moves to competent industry, fabrication, efficient

¹ IICT Telecommunication, University of Sindh, Jamshoro,Sindh, Pakistan

² Shaheed Benazir Bhutto University, Naushahro feroze Campus,Sindh, Pakistan

Corresponding Author: Abubakar2k14@gmail.com

energy management, resource management, health care Management, smarter business take decisions on analyzed data, smart home automation and countless more applications. As this research paper focuses on smart home automation based on IoT, the smart home concept should be understood first. Smart homes combine common devices, found in homes, to be able to control it over the internet. The technology initially was designed and used to control environmental systems, but recently, almost any electrical component can be included within the system of a smart home such as doors, windows, fans, Webcam, etc. [2]. Wide range of articles of The IoT, including items and electric devices that are not generally associated. Cisco predicts that 99% of smart physical appliances will be interconnected. These items contain implanted innovation to collaborate with inward servers and the outside condition. These items are organized competently and can impart over a safe, dependable and accessible system stage. The IoT is based on the associations among the electronic mechanical assembly and things.

3. Aim and Objectives

Using IPv4, OSPF protocols, we aim to remotely control the appliances, which are used in the home, by using IP. We can access it through the internet all over the world. We can implement in the real world because now in the market all Equipment are available which are used for Home Automation. Home appliances are connected through wireless connection and wires. Wireless is best rather than wire because of cost. In this research aims that controlling home appliances via end device using Wi-Fi or cellular network then the end user will directly access through a web-based interface by the web, whereas home appliances like lights, fan and door lock remotely switch [3].

IoT offers a wide scope of new advancements for observing and controlling, of wise structures and keen homes, by upgrading security to lessen vitality and upkeep costs. With the home computerization

control framework, we make our home gadgets shrewd. Savvy as in, the gadgets can be checked or perform the task as indicated by the client's directions. For instance, an entryway lock framework where on the off chance that anybody obscure individual attempts to go into the house without approval, at that point the entryway lock will initiate a caution connected to the entryway and in this we can say our house is keen enough to give us security.

The fundamental target is to interconnect all home appliances with Home gateway via Unguided or guided media to access the internet cloud for controlling and monitoring the home appliances by using API interface.

In this research paper, we focused on home automation and use end devices like cell and computer. The IoT appliances handle and control the electronic electrical and mechanical systems which are used in Homes, institutes, and buildings. The appliances are connected to the cloud server and controlled by a single admin which give the permissions to several users. The admin can approach and control all the nodes connected to each end user but a single end user can control only those appliances to which the user itself is connected [4]. It performs a reality in which we can design this in the real world. We need ISP to connect with the internet and we make a registration server in which every equipment which is using at home registers and we can control remotely.

4. Data Storage

Following are the data storage units:

- 1 KB = (10^3) bytes
- 1 MB = (10^6) bytes
- 1 GB = (10^9) bytes
- 1 TB = (10^{12}) bytes
- 1 PB = (10^{15}) bytes
- 1 EB = (10^{18}) bytes

5. Management of Data

5.1. Structured Data

Structured data is inserted and sustained in a file. Structured data can easily be listed, categorized, reviewed, and evaluated by a computer. For example, in an office you submit employee name, address, salary, and other information to a website, you are creating structured data. Structured data decrease errors and make simpler for the computer to evaluate.

5.2. Unstructured Data

Unstructured data is raw facts and figures. It does not sustain record. So, easily cannot understand unstructured data.

6. IP Addressing

An IP address is a logical address which identifies the device over a computer network. The main task of the IP address are to give an identity of computers and routing of the packets on the network.

6.1. Public address:

A public IP address is an IP address that can be accessed over the Internet. Like postal address used to deliver a postal mail to your home, a public IP address is the globally unique IP address assign to an end device.

6.2. Private Address:

A private IP address is commonly used for local area networks within a building, office, and enterprise environments.

The interconnected network has different sizes. There are many small networks and a few large networks.

In network to provide efficient use of IPv4 32-bit address space, the IPv4 defined several address classes and associated address formats:

Class A: allows 8 bits for the Network portion and 24 bits for the host portion.

Class B: In class, B allows 16 bits for the network portion and 16 bits for the host portion.

Class C: In class, C allows 24 bits for network portion and 8 bits for the host portion.

Class D: Class D is used for multicasting. And

Class E: Class E IP address reserved for research purposes.

7. Network Models

Networking models pattern how data flows within a network. Networking models include:

7.1. Client Server Model

This is the most common model used in networks. Client computer request for service to the server. Servers are often located maybe locally or remotely and managed by the administrator. For example, Microsoft Outlook is a client-server model where end users connect to the email server using a locally installed email client.

7.2. Cloud Computing Model

This is a new model where servers and services are scattered globally in distributed data centers. Synchronized data across multiple servers. Organizations simply subscribe to different services within the Cloud. End users access applications from Cloud servers without requiring an application-specific client. For instance, Gmail email is a cloud service where end-users can access their email from anywhere without requiring a locally installed application. [5]

8. Threats To Physical Safety In IoT

Many IoT devices in the home take part in so-called ‘home automation’ activities and interact with physical world components to make life ‘easier’. However, depending on the nature of the physical world interaction there could be the potential for actual physical safety threats.

For example:

IoT smart meters & thermostats – depending on the level of integration of smart meters with the gas/electricity supply in a

household, remote access to these might give a hacker the opportunity to tamper with temperature levels to dangerously low or high values that could, for example, affect the health of elderly or unwell occupants, or in extreme cases start a fire or gas leak.

- IoT lightbulbs – remote access to these devices might allow for on/off switching which could affect the personal safety of occupants suffering from poor eyesight.
- IoT door lock – the ability to tamper with IoT door locks could affect the safety of occupants living in dangerous neighborhoods or might be used to deliberately lock them in their homes/rooms for nefarious purposes. Previous research by others has shown potential issues with such devices.

9. Wireless Security

The difficulties in keeping a wired network secure are amplified with a wireless network. A wireless network is open to anyone within range of an access point and the appropriate credentials to associate to it. Security and privacy remain a major challenge in IoT [6]. The smart home aim is to enhance the level of intelligence living environment and improves human life [7].

Basic wireless security includes:

- Setting strong authentication protocols with strong passwords
- Configuring administrative security
- Enabling encryption
- Changing all default settings
- Keeping firmware up-to-date

10. System Analysis And Tools

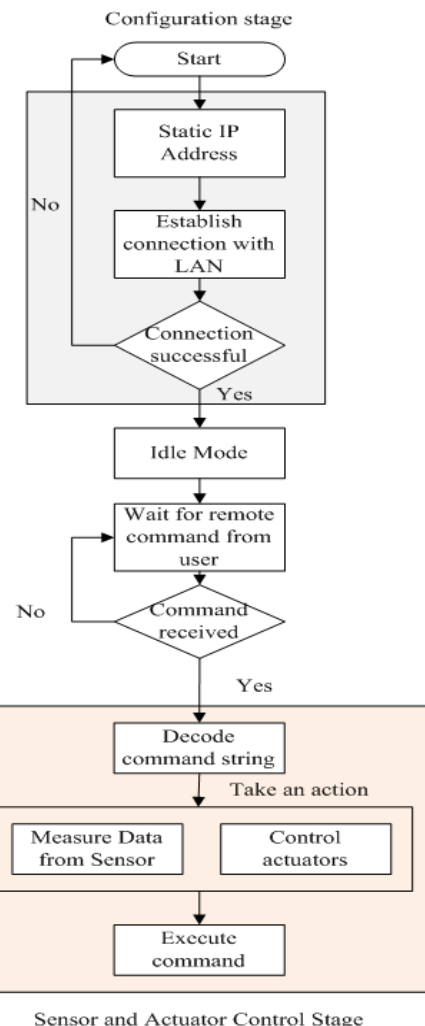


Fig.1 Flow Chart of IoT Based Home Automation

11. Methodology & Implementation

11.1. IoT Based for Home Automation:

There are two major components ISP (Internet Service Provider) and Home Appliances which are connected and accessible through ISP internet.

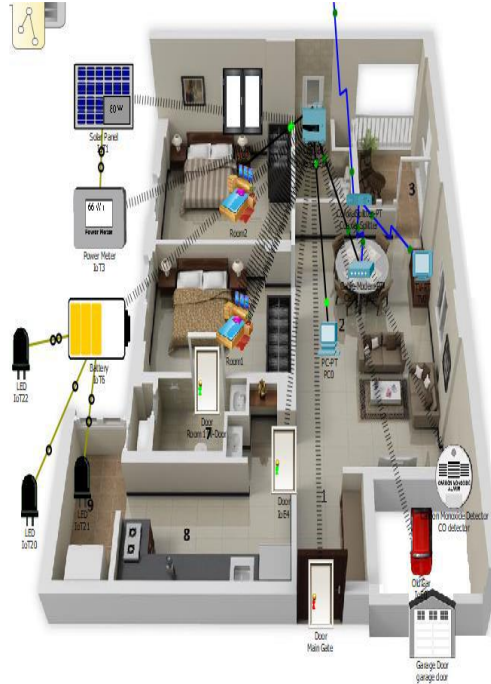


Fig.2 IoT Based for Home Automation Environment

In the home, all appliances are connected & registered with central the home gateway (www.register.com) and the home gateway is connected with ISP. We have reported that the very impressive implementation of the Internet of Things used to monitor the interconnected sensors and transmissions of data via the internet [8]. When Home Gateway Switched "ON", Wi-Fi signal spread in the home covered area & all home appliances can connect after the authentication process. The authentication process successfully completes then automatically IP address assigned by DHCP. If not, then try again.

12. Protocols

12.1. DHCP Protocol:

Dynamic Host Configuration Protocol is used for assigning dynamic IP addresses to the network devices. In DHCP, a device can assign different IP, when the device connects

after switched off. In many systems, the device's IP address can even change while it is still connected. DHCP also provides both static and dynamic IP addresses.

In this research, we prefer to use the OSPF routing protocol for routing of packets in different networks.

12.2. OSPF Protocol:

15.2.1. OSPF Packets: OSPF protocol exchange the routing information packets with neighbor routers and maintain a complete map of the network.



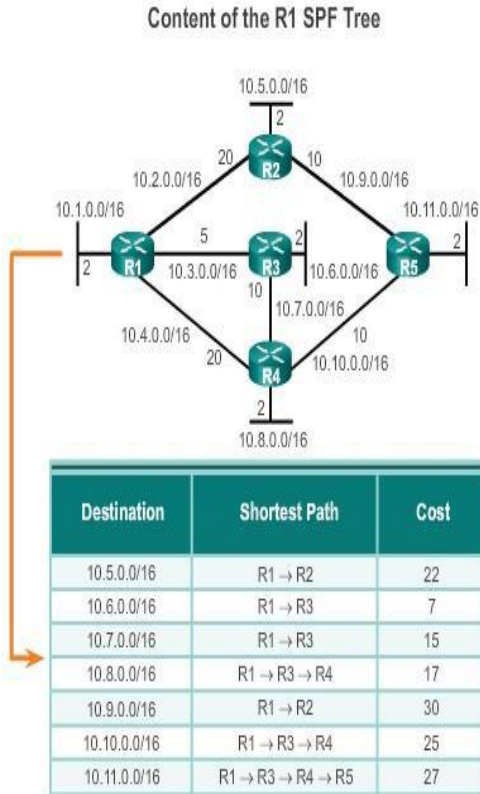
Fig 3. OSPF Packets

15.2.2. If a neighbor is present, the OSPF protocol: Router establishes the neighbor adjacency and creates a routing table.

15.2.3. LSAs keep the state and cost of each directly connected link. Routers flood LSAs to the neighbor. neighbors receiving the LSA immediately flood to other directly connected neighbors to its, until all routers in the area have LSAs.

15.2.4. Build the topology table based on LSAs that received. This database keeps all the information about the topology of the network by using Shortest Path First Algorithm

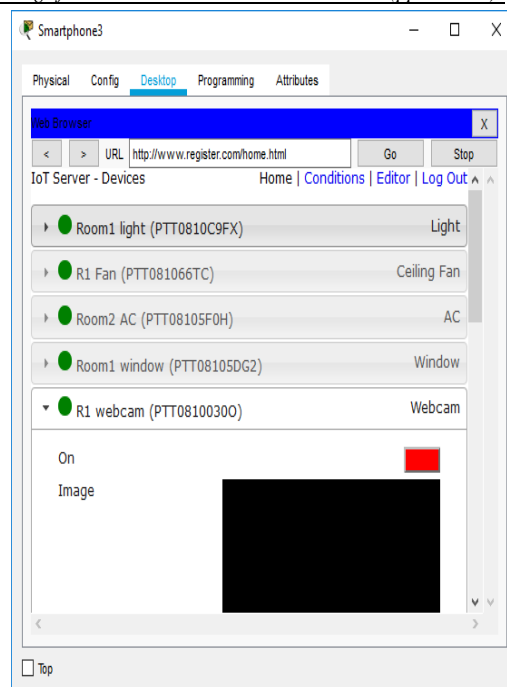
15.2.5. From the SPF database, the best paths are selected and insert into the routing table.

**Fig 4.** Routing Table

13. Results

The appliances which registered with the Server can control remotely through the internet. Steps are given below:

- Step I. Access to the Register Server through a smartphone/end device.
- Step II. Open the web browser and log in with the website (www.register.com) Username and password required for access to Home Appliances.
- Step III. Successfully, login into a register web server then the list of the Home appliances will show in the popup menu. (See figure. 5)

**Fig 5.** Registered List of Home Appliances

- Step IV. And we can switch ON/Off any electronic appliance by web server interface at any time anywhere.

13.1. Practical: 1 CARBON MONOXIDE DETECTOR & THE GARAGE DOOR AUTOMATION

- In the Garage, When Car switched ON, the car emits the carbon monoxide gas and the sensor detects carbon monoxide when it reaches to set level (2) of carbon monoxide gas then the garage door auto opens and closes.

13.2. Practical 2:

- When the motion detector detects the motion inside the room, the Webcam automatically switched “ON” and start to record video and store it into the registered web server. (see figure. 6)

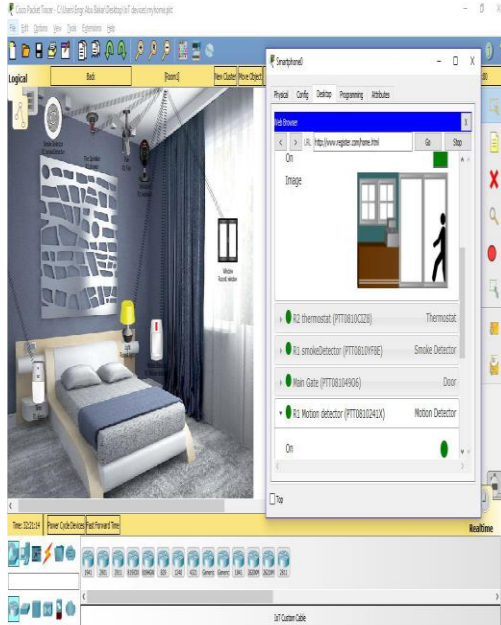


Fig 6. After motion detection

14. Conclusion

The Web-based Internet of Things for home automation has been controlled remotely through a web-based interface. The designed network system not just monitors the sensor information, but also senses the temperature, light, movements as well. For example, Light switched ON when the room gets dark.

Additionally, stores the parameters in the cloud server. This will help, the client user to analyze the state of different parameters in the home whenever anywhere.

All over the world paying attention to IoT, which is the third wave of IT after cellular communication and the Internet. In this paper, we proposed the Web-Based Internet of Things for home automation based on Internet and GPRS that presented the data transmission between wireless sensor networks and cellular mobile networks [9].

ACKNOWLEDGMENT

This research has been conducted at the University of Sindh Jamshoro.

REFERENCES

- [1] Lee, I. and Lee, K., 2015. The Internet of Things (IoT): Applications, investments, and challenges for enterprises. *Business Horizons*, 58(4), pp.431-440.
- [2] Ricquebourg, D., Menga, D., Durand, B., Marhic, L., Delahoche, and C. Loge. The smart home concept : our immediate future. In 2006 1ST IEEE International Conference on E-Learning in Industrial Electronics, pages 23–28, Dec 2006.
- [3] Pavithra, D., and Ranjith Balakrishnan. "IoT based monitoring and control system for home automation." 2015 global conference on communication technologies (GCCT). IEEE, 2015.
- [4] Dey, S., Roy, A. and Das, S., 2016, October. Home automation using Internet of Thing. In 2016 IEEE 7th Annual Ubiquitous Computing, Electronics & Mobile Communication Conference (UEMCON) (pp. 1-6). IEEE.
- [5] Doukas, C. and Maglogiannis, I., 2012, July. Bringing IoT and cloud computing towards pervasive healthcare. In 2012 Sixth International Conference on Innovative Mobile and Internet Services in Ubiquitous Computing (pp. 922-926). IEEE.
- [6] Dorri, A., Kanhere, S.S., Jurdak, R. and Gauravaram, P., 2017, March. Blockchain for IoT security and privacy: The case study of a smart home. In 2017 IEEE International Conference on Pervasive Computing and Communications Workshops (PerCom Workshops) (pp. 618-623). IEEE.
- [7] Feng, Shuo, Peyman Setoodeh, and Simon Haykin. "Smart home: Cognitive interactive people-centric Internet of Things." *IEEE Communications Magazine* 55.2 (2017): 34-39.
- [8] Kelly, S.D.T., Suryadevara, N.K. and Mukhopadhyay, S.C., 2013. Towards the implementation of IoT for environmental condition monitoring in homes. *IEEE sensors journal*, 13(10), pp.3846-3853.
- [9] Zhu, Q., Wang, R., Chen, Q., Liu, Y. and Qin, W., 2010, December. Iot gateway: Bridgingwireless sensor networks into internet of things. In 2010 IEEE/IFIP International Conference on Embedded and Ubiquitous Computing (pp. 347-352). Ieee.

Reactive Power Compensation using Matrix Converter: Indirect Space Vector Pulse Width Modulation Technique

Muhammad Ishaq¹, Muhammad Hammad Afzal¹, Mukhtar Ali¹, Muhammad Waqar²

Abstract:

In this paper, application of matrix converter for the compensation of reactive power is studied. Matrix converter is direct AC-AC converter composed of solid-state bi-directional switches. Space-vector modulation technique is used to control the matrix converter. Simulation are done in MATLAB/Simulink and filters are used to smooth out the output waveforms. Switching frequency optimization is done and its effect on THD and input/output currents/voltages is observed.

Keywords: *Matrix Converter Control, Space Vector PWM, Reactive Power Compensation*

1. Introduction

Reactive power (Q) limits the capacity of a transmission line because it is the unused power. Presence of large amount of Q , consequently, limits the amount of active useful power (P) which can be transmitted across the transmission line. It is therefore, extremely important in power systems to develop a system which can control and reduce reactive power. Higher Q also affects the voltage across the transmission line so this compensation system would also allow to control the voltage of transmission line.

There are many traditional methods to control and compensate reactive power such as FACTs controllers and capacitor banks. Capacitor banks are bulky, heavy and expensive and they also require regular maintenance. FACTs, on the other hand, are

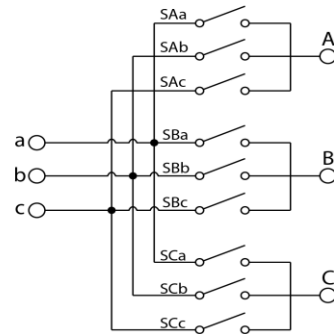


Fig 1:Matrix Converter Schematic
relatively better and more controllable but they still require the use of capacitors, such as in SVC large capacitor is used to handle high voltage [1]. Whereas, in STATCOM smaller electrolytic capacitor is used on DC side.

¹ Department of Electrical Engineering, National University of Computer and Emerging Sciences, H-11/4, Islamabad, Pakistan

² SMME, National University of Science and Technology, H-12, Islamabad, Pakistan
Corresponding Author: muhammadishaq1359@gmail.com

2. Matrix Converter

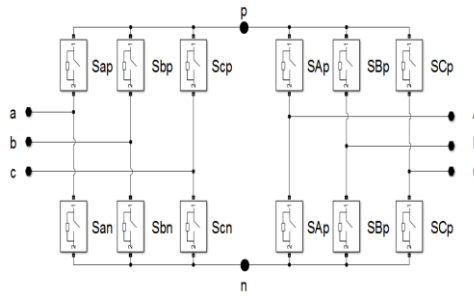


Fig 2:An indirect matrix converter

Reactive power can also be controlled by matrix converter (MC). MC was first proposed by Alesina and Venturini in 1989 [2]. They extensively studied MC and researched on low frequency behaviors of voltages and currents at the output of the system. Earliest difficulties in the research of MC were the commutation of the bidirectional switches [8]. Work around for commutation problems was found by [7] by using intelligent commutations techniques.

MC is direct AC-AC converter as shown in Figure 1. It consists of 9 bi-directional switches and it eliminates the need of intermediate DC-link required in traditional back to back converters. Features of MC includes sinusoidal waveforms at output, control of output amplitude and frequency, compact design due to use of solid-state semiconductor components, Regeneration and unity power factor at input [3].

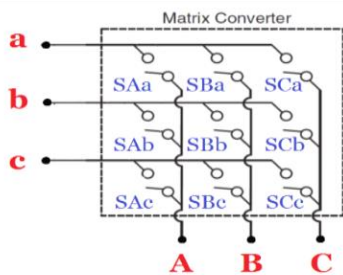


Fig 3: 3x3 Direct matrix converter.

Matrix converter is an ac-ac converter which is arranged in 3x3 array of 9 bi-directional switches. There are two main types of MC topologies: direct and indirect as shown in Figure 2. Indirect MC consists of two stages,

$$\begin{bmatrix} V_a(t) \\ V_b(t) \\ V_c(t) \end{bmatrix} = \begin{bmatrix} S_{Aa}S_{Ba}S_{Ca} \\ S_{Ab}S_{Bb}S_{Cb} \\ S_{Ac}S_{Bc}S_{Cc} \end{bmatrix} * \begin{bmatrix} V_A(t) \\ V_B(t) \\ V_C(t) \end{bmatrix} \quad (1)$$

$$\begin{bmatrix} i_a(t) \\ i_b(t) \\ i_c(t) \end{bmatrix} = \begin{bmatrix} S_{Aa}S_{Ab}S_{Ac} \\ S_{Ba}S_{Bb}S_{Bc} \\ S_{Ca}S_{Cb}S_{Cc} \end{bmatrix} * \begin{bmatrix} i_A(t) \\ i_B(t) \\ i_C(t) \end{bmatrix} \quad (2)$$

first is rectification stage and second is inversion stage. An imaginary dc-link is assumed between these two stages for the purpose of modulation of MC [4]. Relationship between input and output voltage and current is represented by (1) and (2).

Table I: 27 Switching states of Direct Matrix Converter.

No	Aa	Ab	Ac	Ba	Bb	Bc	Ca	Cb	Cc
1	1	0	0	0	1	0	0	0	1
2	0	1	0	0	0	1	1	0	0
3	0	0	1	1	0	0	0	1	0
4	1	0	0	0	0	1	0	1	0
5	0	1	0	1	0	0	0	0	1
6	0	0	1	0	1	0	1	0	0
7	1	0	0	0	1	0	0	1	0
8	0	1	0	1	0	0	1	0	0
9	0	1	0	0	0	1	0	0	1
10	0	0	1	0	1	0	0	1	0
11	0	0	1	1	0	0	1	0	0
12	1	0	0	0	0	1	0	0	1
13	0	1	0	1	0	0	0	1	0
14	1	0	0	0	1	0	1	0	0
15	0	0	1	0	1	0	0	0	1
16	0	1	0	0	0	1	0	1	0
17	1	0	0	0	0	1	1	0	0
18	0	0	1	1	0	0	0	0	1
19	0	1	0	0	1	0	1	0	0
20	1	0	0	1	0	0	0	1	0
21	0	0	1	0	0	1	0	1	0
22	0	1	0	0	1	0	0	0	1
23	1	0	0	1	0	0	0	0	1
24	0	0	1	0	0	1	1	0	0
25	1	0	0	1	0	0	1	0	0
26	0	1	0	0	1	0	0	1	0
27	0	0	1	0	0	1	0	0	1

(1) relates input voltage with output current whereas (2) relates output current with input current.

- 18 active vectors (two output lines connected to one input terminal, the third line to another terminal one input terminal is not connected).

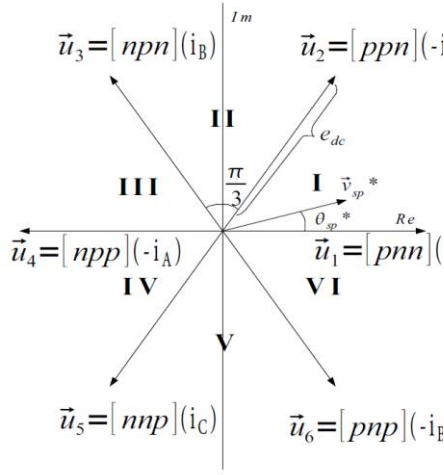


Fig 4: VSI stage voltage space-vectors in complex plane.

Direct MC has 9 switches. Therefore, total $2^9=512$ switching combinations are possible. But these combinations are further constrained by following rules [5]:

- Two Input terminals cannot be short circuited.
- An output terminal cannot be left open.

These rules can be expressed by following equations [4]:

$$S_{Aa} + S_{Ab} + S_{Ac} = 1 \quad (3)$$

$$S_{Ba} + S_{Bb} + S_{Bc} = 1 \quad (4)$$

$$S_{Ca} + S_{Cb} + S_{Cc} = 1 \quad (5)$$

27 switching combinations are categorized into three parts [5]:

- 3 zero vectors (all output lines connected to a same input terminal).
- 6 rotating vectors (every output line connected to a different input terminal).

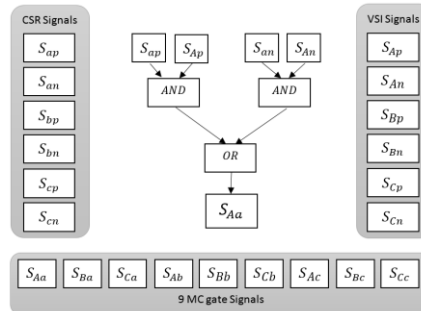


Fig 5: Transformation of 12 gate signals into 9.

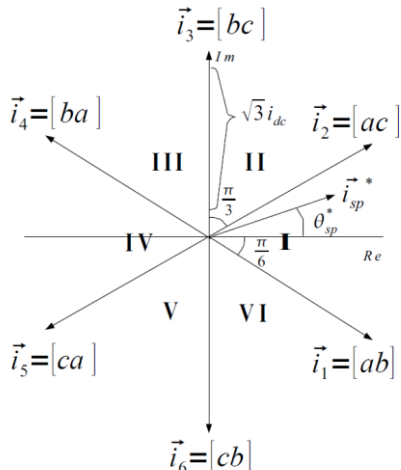


Fig 6: CSR stage current space-vectors.

3. Control Scheme For Matrix Converter

In this research direct topology of matrix converter will be used for simulation but for modulation, indirect matrix converter will be assumed in which first stage will be modulated as current source rectifier (CSR) and second

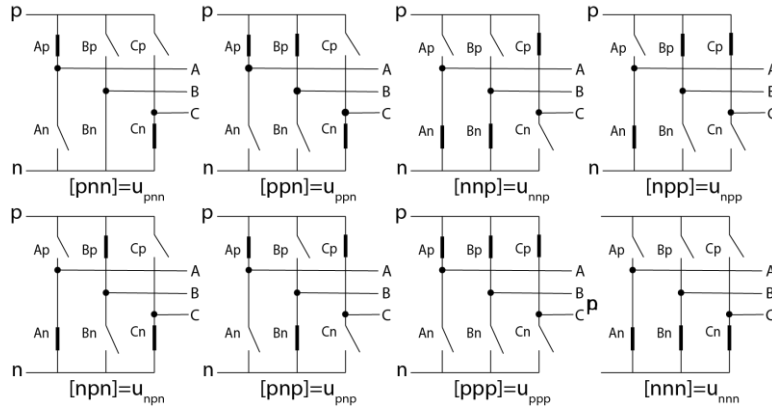


Fig 7: Switching states of VSI stage.

stage will be modulated as voltage source inverter (VSI) [6].

Voltage and current space vectors are shown in Figure 4 and 5 respectively. Control scheme outputs 12 gating signals, 6 signals for CSR namely Sap, San, Sbp, Sbn, Scp, Scn and 6 signals for VSI namely SAp, SAN, SBp, SBn, SCP, SCn. Conversion from 12 gating signals to 9 signals such as SAa, SA_b, SA_c, SBa, SB_b,

SC_b, SC_a, SC_b, SC_c, is done by the process demonstrated in Figure 6.

A reference input is given to each control stage such as current reference for CSR and voltage reference for VSI. There are $23 = 8$ switching states of VSI because two switches in one leg cannot be closed simultaneously. There are 6 active vectors as shown in figure 5 and other two are called zero vector where

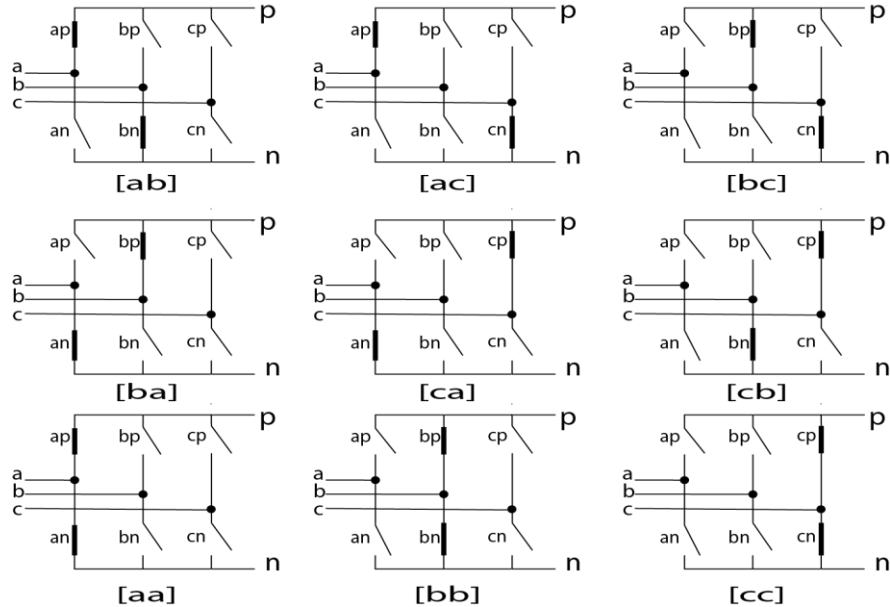


Fig 8: Switching states of CSR stage.

either all positive terminal switches or all negative terminal switches are closed. Expression (6) and (7) represent voltage and

$$\vec{v}_{sv} = \frac{3}{2} \vec{V}_0 e^{j\omega t} = \frac{3}{2} q \vec{V}_i e^{j\theta_{sv}} \quad (6)$$

$$\vec{i}_{sv} = \frac{3}{2} \vec{I}_i e^{j\theta_{sv}} \quad (7)$$

current space vectors [7].

where q is modulation index and $\theta_{sv} = \omega t - \varphi_i$, and φ_i is input displacement angle which is required to be controlled to reduce reactive power. The expression for virtual dc link is given in (8).

$$e_{dc} = \frac{3}{2} \frac{\vec{V}_i \vec{I}_i \cos \varphi_i}{i_{dc}} = \frac{3}{2} \vec{V}_i \cos \varphi_i \quad (8)$$

e_{dc} is dc link voltage and it is also the length of all active vectors.

Reference vectors rotate in fig 4 and 5 with angular velocity of ω . Reference vectors are formed by 2 closely located active vectors and a zero vector [6].

Where T_{a1} is time duration of application of first active vector and similarly T_{a2} for second active vector and T_z for zero vector. T_s is sampling time.

4. Simulation Results

Two systems as shown in fig 9 are simulated, one with matrix converter and one without it. From these simulations, it can be

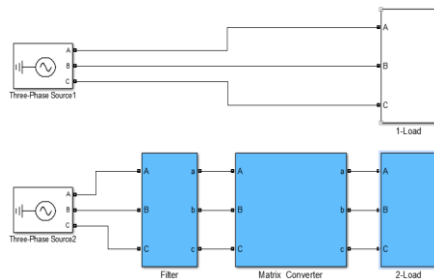


Fig 9: Simulation Diagram.

observed that using matrix converter to control the input displacement angle results in reduced reactive power in the system. Figure 10 shows voltage and current waveforms of system where reactive power control has not been implemented, here the displaced angle is about 51 degrees.

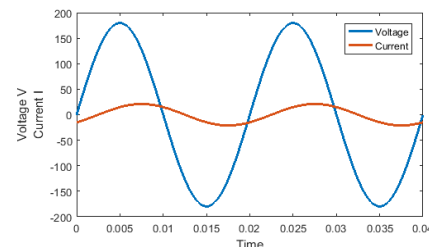


Fig 10: Displacement between voltage and current without matrix converter.

$$T_{a1} = T_s \frac{3qV_i \sin\left(\frac{\pi}{3} - \theta_{sv}\right)}{e_{dc} \sin\left(\frac{\pi}{3}\right)}$$

$$T_{a2} = T_s \frac{3qV_i \sin(\theta_{sv})}{e_{dc} \sin\left(\frac{\pi}{3}\right)}$$

$$T_z = T_s - T_{a1} - T_{a2}$$

Figure 12 shows output voltage and current at two different frequencies i.e 5000 Hz and 10000Hz. Although increasing switching frequency improves the output current waveform, it increases total harmonic distortion (THD) in output voltage. So, a tradeoff is found between switching frequency and acceptable amount of THD in Figure 11. Figure 13 shows input voltage and current waveform while using matrix converter to control displacement angle. It can be observed from the figure that current closely follows voltage resulting in reduced reactive power. Figure 14 shows improvement in smoothness of input current waveform when an input filter is used.

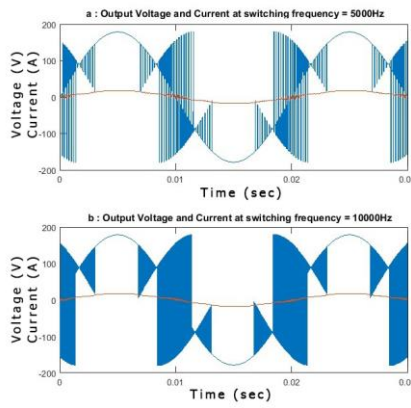


Fig 12: Output voltage and current after using filter.

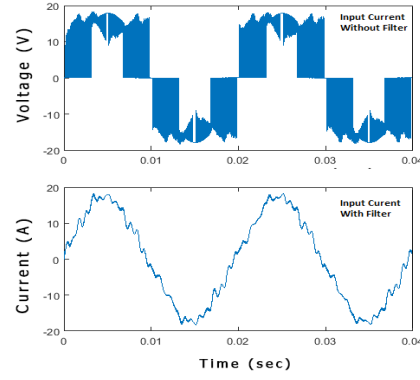


Fig 14: Input current after using filter.

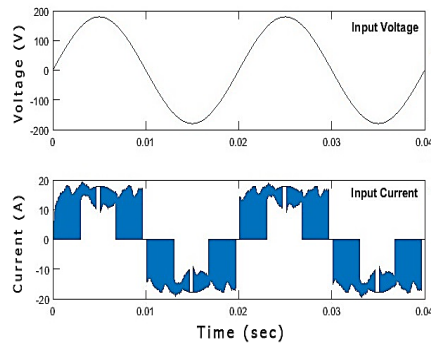


Fig 13: Input Voltage and Current waveforms of MC.

Different switching frequencies are tested to find a range of different switching to reduce power losses as well as total harmonic distortion of signals. It can be observed in figure 11 that range of switching frequency between 5000Hz to 7000Hz is sufficient because increasing frequency beyond this point don't have any significant effect on THD.

5. Conclusion

In conclusion, Space Vector pulse width modulation technique (SVPWM) is indirectly applied to a 3x3 direct matrix converter (DMC). Simulation performed in Simulink are presented. This system of Matrix Converter has capability of performing in wide variety of situations and yield consistent results. Reactive power compensation is achieved by using inductive load. Any type of load can be used such as inductive or capacitive. Output waveforms are affected by distortion due to switching of bidirectional switches, this total harmonic distortion is reduced to an optimum level by extensively studying wide range of switching frequencies.

REFERENCES

- [1] K. Padiyar, FACTS Controllers in Power Transmission and Distribution, New Age International Publishers, 2007.
- [2] K. Hulusi and A. Ramazan, "Control of Venturini Method Based Matrix Converter in Input Voltage Variations," International MultiConference of Engineers and Computer Scientists, 18-20 03 2009.

- [3] S. Pawel, Three-phase AC-AC Power Converters Based on Matrix Converter Topology, Springer, 2013.
- [4] H. Nathelie and M. Marta, "Reactive Power Compensation using an indirectly Space Vector-modulated Matrix Converter," IEEE International Symposium on Industrial Electronics (ISIE), pp. 2455-2460, 08 2010.
- [5] R. Jose, R. Marco, K. Johan and W. Patrick, "A Review of Control and Modulation Methods for Matrix Converters," IEEE TRANSACTIONS ON INDUSTRIAL ELECTRONICS, pp. 58-70, 01 2012.
- [6] B. Kuldeep and B. Subrat, "A Novel Control Strategy of Indirect Matrix Converter Using Space Vector Modulation," International Journal of Power Electronics and Drive System (IJPEDS), vol. 03, no. 07, pp. 926-935, 2016.
- [7] O. Khaled, D. Mohamed and J. Mohamed, "A SVM Control Strategy for a Direct Matrix Converter," IEEE TRANSACTIONS ON POWER ELECTRONICS , pp. 1-10, 2013.
- [8] L. Zhang, C. Watthanasarn, and W. Shepherd, "Control of AC-AC matrix converters for unbalanced and/or distorted supply voltage," in Proc. 32nd Annu. IEEE Power Electron. Spec. Conf., 2001, vol. 2, pp. 1108–1113.

Review on SCR catalysts by focusing impacts of sulfur on SCR performance

Ghazanfar Mehdi¹, Song Zhou¹, Yuanqing Zhu¹, Zubair Ali Shah¹, Kishore Chand², Raza Waleed³, Asif Raza⁴, Sanaullah⁴

Abstract:

Marine diesel engines are extensively used for transportation and as well as for power generation purpose because of its higher durability, thermal and fuel efficiency than the gasoline engines. But the marine diesel engine produced severe NOx emissions that are currently well discussed issue needed to be solved due to its serious health and environmental problems. At the same time, because of increasing stringent regulations of NOx emissions it is necessary for ships to meet the international maritime organization (IMO) Tier III regulations in NOx emission control areas (ECA). It is enforced for the vessels that are constructed on and after the 1st January 2016. Therefore, a demand for well-functioning NOx reduction technology is required. Currently SCR is the most dominant and mature technology used to reduce the NOx with ammonia over the SCR catalyst. SCR catalyst is the core part of SCR system; hence this review described the different types of catalysts and their behavior under different conditions. Furthermore, the deactivation of SCR catalyst occurs by different mechanisms; however, the most significant mechanism is sulfur poisoning. Reaction temperature and availability of ammonia is also significant parameter for sulfur poisoning. Therefore, it is necessary to investigate how sulfur behaves with SCR catalysts. Even though many studies have been performed on Sulphur poisoning of catalysts but still requires complete understanding. This review covers the sulfur poisoning of vanadium and Cu-zeolites based SCR catalysts with mainly focus on Cu-zeolites because of its sulfur sensitivity.

Keywords: marine diesel engine, selective catalytic reduction; vanadium; cu zeolite; sulfur

1. Introduction

Because of their high thermal efficiency and durability, marine diesel engines are

extensively used for power generation as well as for transport purpose. However, only transportation sectors are producing almost world's 30% greenhouse gases [1]. Marine diesel engine emissions produced serious

¹ College of Energy and Power Engineering, Harbin Engineering University, Harbin 150001, China

² College of Material science and Chemical Engineering, Harbin Engineering University, Harbin 150001, China

³ College of Underwater acoustic Engineering, Harbin Engineering University, Harbin 150001, China

⁴ College of Mechanical and Electrical Engineering, Harbin Engineering University, Harbin 150001, China

Corresponding Author: ghazanfarmehdi22@gmail.com

environmental hazardous gases specially NO_x . The carbon monoxide (CO), carbon dioxide (CO_2) and hydrocarbon (HC) exhaust emissions is much lower in marine diesel engines, as in comparison to automobile design engines and on the contrary, it produces more detrimental Nitrogen oxides (NO_x) emissions [2]. NO_x emissions are produced due to the combustion process of diesel engine. There are three main sources of NO_x formation named as thermal NO_x , fuel NO_x and prompt NO_x . The involvement of fuel NO_x and prompt NO_x to the total NO_x emissions is negligible [4]. Basically thermal NO_x is the major contributor of NO_x formation throughout the whole combustion process [3]. NO_x is very noxious, hazardous and it creates an irritation. It is responsible for the headache and nausea [5]. NO_x can react with existence of sunlight and other organic compounds to form ozone layer. In the troposphere Ozone is named as ground level ozone. When NO_x is reacted with water, nitric acid can be formed which is the major source of acid rain [6]. In order to reduce NO_x from ships, many national governments and international organizations in the world have promulgated different regulations on shipping emissions, and also enforced strict requirements on NO_x emission in the Emission Control Areas (ECA) [7]. In 2016, IMO Tier III standard on NO_x emission proposed by International Maritime Organization (IMO) has already been enforced in North America Emission Control Area (ECA), including the East and West coast of the USA and Caribbean [8]. Due to the increasing stringent emission regulations, it is necessary for vessels to meet the IMO Tier III legislations applied for ships constructed on and after the 1st January 2016 in NO_x emission control areas. Fig. 1 represents the limits of NO_x legislations. It is enforced that, during the operation of ships NO_x emissions should not exceed 3.4g/kWh. In the requirement of Tier III NO_x emission decreased up to 75% as compared to IMO Tier II [9].

Currently three most mature technologies such as exhaust gas recirculation (EGR),

Selective catalyst reduction (SCR) and dual fuel are mostly used worldwide to control the NO_x as shown in Fig. 2 [10]. It has been observed that in order to decrease the NO_x emission intensely and meet the requirements of IMO Tier III, SCR, EGR and Dual fuel can be the effect methods. SCR and EGR are the most feasible and mature techniques used to decrease the NO_x of two stroke marine diesel engines. But the dual fuel is not good

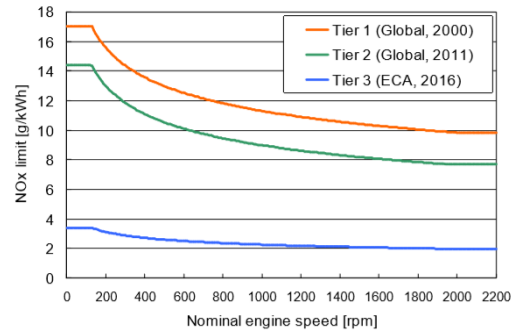
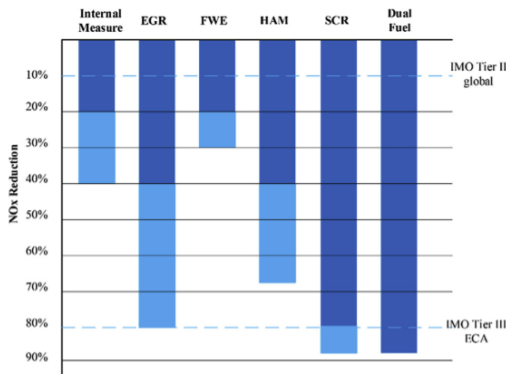


Fig. 1. Represents the limits of NO_x legislations [9]

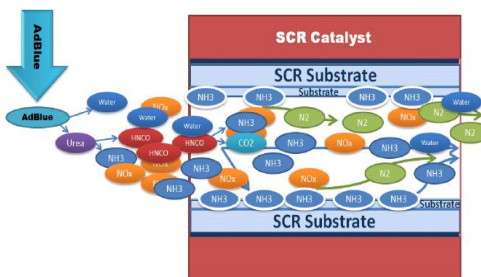
option, because the low speed two stroke marine diesel engines are still using HFO (Heavy Fuel Oil). But SCR in comparison to EGR is the front runner technology in marine diesel engine due to its higher DeNO_x efficiency [11]. In EGR system NO_x can be reduced by diverting the exhaust flow of burned gases into combustion chamber. As the recirculated burned gas entered, it is responsible for lowering the adiabatic flame temperature.

Due to the lowering of in-cylinder temperature NO_x formation has been reduced. But as a result of temperature reduction, the efficiency of engine also decreased which tends to increase the fuel consumption. Therefore, SCR is the most

**Fig. 2.** NO_x Removal Technologies

prominent and leading technology because it operates with higher efficiency without compromising on both flame temperature and NO_x conversion [12].

SCR is the dominant technology used to meet the most recent emission standards due to its technical maturity, better fuel economy and low cost for the emission reduction. SCR is means of converting NO_x into N₂ and H₂O by using catalyst and oxygen (O₂) [13]. However, pressure drop occurs at SCR catalyst therefore more efficient turbocharger is necessary for SCR system.

**Fig. 3.** Systematic representation of SCR System

As the NO_x is decreased into N₂, between the temperature ranges of 300 - 400 °C, the load of engine must be 40% and above. Ammonia (NH₃) will start burning when the exhaust temperature of engine goes beyond the 400 °C which will make the system ineffective. SCR catalyst reaction will become slow and undesirable reactions such as formation of ammonium sulfates will occur when the

temperature goes below 270 °C, which ultimately destroy the catalyst. Therefore, SCR reaction is mainly restricted by the catalyst activity, species concentration and reaction temperature [14]. Fig. 3 shows the systematic representation of SCR system.

2. Challenges related to SCR system

The major challenges involved with SCR systems is the reduction of catalytic converter volume at low temperatures and the suitable dosing strategy for NH₃ at frequently varying load conditions of the diesel engines. Additionally, the risk associated concerning storing and handling of gaseous NH₃ is significant and consequently it is not commonly used as a reducing agent directly. For reasons of toxic nature of NH₃, handling and storing problems, urea is the preferred substitute for NH₃ as a reducing agent in automotive applications. The best procedure is injecting Urea Water Solution (UWS) in the form of spray to hot exhaust stream before the entry to the SCR catalyst [15]. Urea is an environmentally benign chemical which makes it more suitable for application of the SCR process. Urea is a fertilizer used in agriculture and available in a number of quality grades at a lower cost. Development of Urea-SCR over NH₃-SCR has gained momentum due to various problems involved with the use of NH₃. NH₃ is corrosive, toxic in nature and also a secondary pollutant. In order to introduce NH₃ into the exhaust gas stream, proper dosage control mechanism is required [16].

The main advantage with this SCR system is high De-NOx efficiency (90% or higher). The disadvantages involve the space required for the catalyst, high capital and operating costs, formation of other emissions (NH₃ slip) and formation of undesirable species which may lead to catalyst poisoning and deactivation. The NH₃ slip can be controlled by installing an oxidation catalyst after the SCR system. Although the SCR system has some drawbacks, the technology has been chosen by the majority of the diesel engine manufacturers due to absence of better technology to meet the stringent emission standards [15].

There are two main objectives related to SCR system.

- To minimize the NO_x emissions
- To minimize the ammonia slip

Following factors should be controlled to get the maximum output in above two objectives.

- Design optimization
- Control system
- Temperature fluctuations
- Low operating temperature
- Poisonous species present in the catalyst
- Mechanical vibrations
- Flow variations

Throughout the low load operating conditions, exhaust temperature is also low; this will put direct effect on the chemical reaction of SCR catalyst, which makes reaction slow at low temperature for characteristic composition of exhaust gas. Variations of engine load influenced the flow rate of exhaust gas, temperature, and composition of exhaust gases. Therefore, it is necessary to control the above factors to improve the NO_x conversion and to reduce the ammonia slip. In general, there is trade off relationship in between NO_x reduction and ammonia slip [17].

3. Research evolution of SCR catalyst

Catalyst is the core part of SCR system. It has been used for reducing the activation energy, NO_x decomposition temperature during reaction, to avoid the incidence of unwanted reactions, increase the amount of N₂ in production side and by this means reaction efficiency has been improved. Catalysts selection is the most important. Particularly, the competent SCR catalysts possessed the characteristics as listed below:

- DeNO_x ability should be high
- Anti-poisoning capacity should be high
- Strong mechanical strength
- Operating temperature should be proper.

3.1. Vanadium based SCR catalysts (VSCR)

A VSCR catalyst is the established technology, mostly used in mobile applications [18]. It is the cheapest of all SCR catalysts [19] and also well known for sulfur tolerance [20]. VCRs operates approximately in the temperature range of 280-500 °C [19, 21, 22]. It is also used at low temperatures, but as a result low NO_x removal efficiency occurs. A VSCR catalyst is mainly composed with the mixture of WO₃/V₂O₅/TiO₂, where, WO₃ is the thermal promoter and used to increase the catalyst acidity, V₂O₅ is worked as an active component and TiO₂ is added as a carrier material [20].

The main disadvantage of VSCR is the sudden decline in the performance of acidity and selectivity at the higher temperatures. Deterioration of catalyst or alkali poisoning starts when the temperature window in between of 550-600 °C [18]. Toxicity of vanadium species is also an important issue [19].

3.2. Cu-zeolites based SCR

During the last few years, Cu-zeolites based SCR catalysts becomes the most preferred catalyst because of its high performance [19]. It is commonly used in movable applications [23]. The key benefits related to Cu-zeolites based SCR catalysts are the hydrothermal stability and higher NO_x activity within the temperature window of 150 to 600 °C [24]. Cu-zeolites based SCR catalysts have good performance even at low temperatures and it is also less sensitive on activity because of the NO₂ Concentration variations [19]. However, Cu zeolites are recognized for their higher sensitivity towards sulfur than the vanadium-based catalysts [25]. A MFI framework of Cu/ZSM-5 was first discovered in 1986, as an effective catalyst used for SCR system [26]. Currently, keen interest is showed towards catalyst structure based on the small pores; with special focus on the Cu/SAPO-34 and on Cu/SSZ-13. Both catalysts have chabazite type structure but the composition of elements is different. While Cu/SAPO-34

is silicoaluminophosphates and Cu/SSZ-13 are zeolites [27]. While comparing the small pore structure of zeolites catalyst with the structure of larger pore, the structure with small pores has been observed more hydrothermally stable. Besides a very high NO_x activity and selectivity can be achieved. Furthermore, less amount of by products such as N₂O can be formed during operating temperature range [27] and also it is less vulnerable for hydrocarbon poisoning [19].

While the comparing of Cu/SAPO-34 and Cu/SSZ-13, it was observed that Cu/SAPO-34 has been more hydrothermal stable rather than Cu/SSZ-13 [26].

A number of catalysts proved to be suitable in favor of SCR reactions. The most important proper components are transit oxides of metal, although Al₂O₃, zeolite, TiO₂, SiO₂ and carbon are frequently used

Table I. Summarized description of main SCR catalysts

Type of catalysts	Proper components	Carrier	Advantages	Disadvantages	Ref:
Commercial catalyst based on vanadium titanium	V ₂ O ₅	TiO ₂	SO ₂ resistance is high, SCR activity at high and low temperature	Oxidation of SO ₂	[28-30]
Noble metals	Sn, Ag, etc.	TiO ₂ , Al ₂ O ₃ etc.	H ₂ O and SO ₂ resistance is high; high low temperature SCR activity	Narrow temperature window; high cost; generation of NO ₂ ; ammonia oxidation	[31, 32]
Oxides of metal	V ₂ O ₅ , CuO, CeO ₂ , MnO _x , CoO _x , FeO _x , and other composite oxide.	TiO ₂ , Al ₂ O ₃ etc.	SCR activity is high at 300-400 C; thermal stability is good; poisoning resistance is high	Poor activity at low temperatures	[33, 34]
Zeolite	Mn, Ce, Fe, Co, Cu, Cr, etc.	Zeolite	Wide temperature window	Hydrothermal stability is poor	[35, 36]
Carbon catalyst	V ₂ O ₅ , CeO ₂ , MnO _x , etc.	Active carbon, Active carbon filter, carbon nanotubes	Easy regeneration, Specific surface area is large, chemical stability is high, high low temperature activity	Poor SO ₂ resistance; energy consumption is high; frequent regeneration.	[37, 38]

like carriers. All catalysts have possessed different advantages and disadvantages and DeNO_x properties, which have been described in table. 2.

3.3. Catalyst Deactivation

The selectivity and activity loss of catalyst over time is known as catalyst

deactivation. Mostly there are three mechanisms for the deactivation of SCR catalysts named as thermal, chemical and mechanical. These mechanisms of catalyst decay can be further elaborated into six sub-mechanisms where thermal decay by thermal deprivation such as fouling, sintering and poisoning. Chemical decay can happen due to

vapor formation, solid-solid reactions and poisoning. Mechanical decay can occur through crushing or fouling. The most important mechanisms for catalyst deactivation are poisoning and fouling [39].

When poisoning is strong, gas-surface chemisorptions happen on catalyst surface; hence, as a result, it blocks the sites for catalyst reaction. Poisoning of species depends upon the adsorption strength of species. The poisoning of species is either produced due to the change in the electronic

or geometrical structure of surface or it just blocks the adsorption sites physically. The poisoning of species can be slow or fast, it mostly depending upon the concentration of poison. It can be irreversible or reversible depends upon the adsorption strength of poison [39]. Fouling is due to deposition of species physically produced from fluid phase over the catalyst pores and in the catalytic surface. This is responsible for the blockage of pores and sites, which ultimately result in the loss of activity of catalyst [39].

4. Sulfur poisoning of SCR catalysts

Deactivation of SCR catalyst occurs by different mechanisms; however, the most significant mechanism is sulfur poisoning. The important factor that influences the sulfur poisoning is the type of catalyst material. Some are more and some are less sulphur tolerant depending on the catalyst materials. Reaction temperature and availability of ammonia is also significant parameter for sulfur poisoning. Therefore, it is necessary to investigate how sulfur behaves with SCR catalysts. Although many studies have been done on sulfur poisoning of catalysts, still it requires complete understanding. This review covers the sulfur poisoning of vanadium-based catalyst and Cu-zeolites SCR catalysts with mainly focus on Cu-zeolites because of its sulfur sensitivity.

Many studies present in this review are to investigate the impact of sulfur on SCR activity by accelerating the lab aging in flow reactors. The accelerated aging in lab has been carried out by using the different catalysts for sulfur under different conditions. There are different sulfation methods named as SO₂ exposure in the presence of ammonia, SO₂ exposure under different SCR conditions or SO₃ exposure at different temperature ranges. Few studies also related to the investigation of sulfur poisoning through experimental setup by using fuel with high sulfur contents. The experimental setup which is mostly used to investigate the sulfur

4.1. Sulfur in exhaust gases

The main source of sulfur at the diesel exhaust is originated from the engine lubricating oil and the presence of sulfur contents in the fuel [40]. Throughout the last few years, contents of sulfur present in diesel fuel decreased extensively. Hence, as a result, SO₂ level reduced in the atmosphere and also to avoid the use of highly efficient aftertreatment system at the diesel exhaust which is more sulfur sensitive. Today, In North America and Europe Ultra-low sulfur diesel (ULSD) fuel is used which contains sulfur contents less than 10-15 ppm [41]. At diesel exhaust, sulfur oxides (SO_x) concentration depends upon the air fuel ratio and contents of sulfur present in the diesel fuel, this relation is represented in Fig 4 [42]. Sulfur is mostly in the form of SO₂ at the exhaust of diesel engine. It can be further oxidized into SO₃ when the SCR system is located beyond the diesel oxidation catalyst (DOC) [40].

4.2. SCR operated on Heavy Fuel Oil (HFO)

Heavy fuel oil (HFO) is well known for its challenges and disadvantages related to SCR system because it contains high sulfur contents in the diesel fuel. Therefore, it allows the oxidation of SO₂ to SO₃ during the SCR reaction. It is responsible for the formation of white plumes and Ammonium Bi sulfate (ABS). Furthermore, with the use of HFO the natural contents of vanadium-based catalysts result in the prominent oxidation of SO₂. Therefore, at present it is

necessary to design the SCR system in a way that resists the unwanted side reactions.

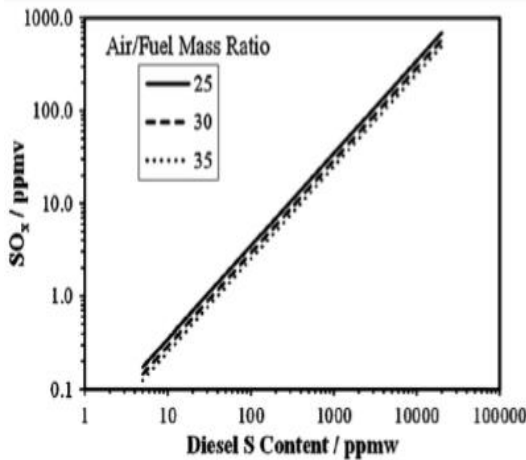
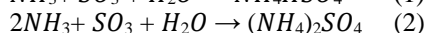
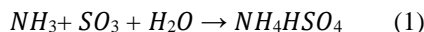


Fig. 4. Relation in between the contents of sulfur in the diesel fuel and SO_x concentration at diesel exhaust for three air to fuel ratio

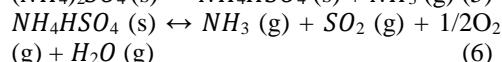
In two-stroke diesel engines, because of the high energy efficiency, the temperature of gases at the diesel exhaust is low after the turbocharger. It is in between of the 230–260 °C depending upon the load of the diesel engine. Low temperature at diesel exhaust creates problem for the SCR system when the HFO is used in the diesel engine. Hence, in order to get the high fuel flexibility, the main precedence of diesel engine is to produce the exhaust gases with suitable temperature window, which ultimately results in improving the SCR system. The exhaust gas temperature around 330 to 350°C should be ideal during the working of engine on HFO [43].

4.3. Formation of ammonium sulfates

Ammonium sulfates are produced when the exhaust temperature is low during the SCR catalyst reaction in the presence of NH₃ and SO_x as shown in reactions below:



Ammonium bisulfate (ABS), NH₄HSO₄ and Ammonium sulfate (NH₄)₂SO₄ are responsible for the physical blockage of pores and channels of catalyst. Therefore, the result in the deactivation of catalyst. ABS is the most hazardous of all the species [44]. ABS is generally formed, when the temperature is in between 190–240 °C and it starts to decompose when temperature goes around 350 °C [45]. The (NH₄)₂SO₄ decomposition occurs in two stages, first it decomposed into NH₃ and NH₄HSO₄ at about temperature of 300 °C as represented in reaction 5. Second, NH₄HSO₄ will start decomposing when the temperature reaches at higher level as shown in reaction 6 [46].



4.4. Impacts of Sulfur on vanadium based SCR catalyst

Many authors have proved that, vanadium-based catalysts are operated at relatively narrow temperature range (300–400 °C) of SCR system [47, 48]. If the operating temperature goes below to the 320 °C, the sulfur poisoning, specially poisoning of SO₂ becomes more imperative and the selectivity and activity of the SCR catalysts decreases, significantly. Furthermore, when the temperature goes above to the 400 °C, undesirable side reactions can occur which are responsible to produce N₂O and NO from the oxidation of NH₃ [49]. NO_x removal efficiency is decreased progressively by means of catalyst aging. Presence of SO₂ can cause the deactivation of SCR catalysts during the SCR operation. Inhibition of SO₂ is the most common problem during the activity of catalyst [47, 50, 51]. Following poisoning mechanism of SO₂ is imagined when NH₃-SCR process is used. On the catalyst surface, SO₂ can be oxidized into SO₃. The produced SO₃ reacts with NH₃ to generate the unwanted reactions such as (NH₄)₂SO₄ and NH₄HSO₄. These two generated undesirable substances deposit in the pores of SCR catalyst, which deactivate

and block the active sites and cause the rapid decrease in the catalyst surface area [52].

The conversion rate of SO₂ is vary from 1%–2% during the normal operating conditions of SCR system [53]. Many studies have proved that, in vanadium-based catalyst V=O bond shows the important role in the oxidation of SO₂ [54]. Thus, the content of V₂O₅ is generally set to be smaller in the SCR catalyst in order to avoid the generation of SO₃. Water vapors appear in the flue gases and can be condensed on the surface of catalyst. It not only produces the exacerbate poisoning by the alkali metals like Na and K, but also responsible for the vaporization and swelling with the increase of temperature. It damages the structure of catalyst, hence in result SCR catalyst is cracked.

It has been reported that for the physical adsorption water vapor is to compete with NH₃ and NO on the surface of catalyst, by this means deNO_x activity of catalyst decreased [55].

The alkali metals such as (Na, K) available in fly ash also disgrace the performance of catalyst when they deposited in the catalysts. Therefore, lengthy acquisition can block pores, which results the poisoning of catalyst [51].

4.5. Impact of sulfur on Cu-zeolite SCR catalyst

Cu-zeolites are the more sulfur sensitive than vanadium-based catalysts. In this review catalysts with small pores such as Cu/SSZ-13 and Cu/SAPO-34 belong to chabazite family are concerned. The exposure of SO₂, SO₃ and/or SO₂ + NH₃, SO₂ are investigated at different conditions of sulfur poisoning, also by considering the impact of temperature simultaneously.

4.5.1. Impact of sulfur on SCR chemical reactions

The different SCR reactions have different impact on the sulfur poisoning of Cu-zeolites catalysts. Standard SCR reaction is much affected than the fast SCR reaction [56, 57]. Furthermore, at low temperatures catalyst activity is severely impacted than the catalyst activity at high temperatures [58].

4.5.2. SO₂ impact on SCR catalyst activity

Many studies have shown the deactivation of Cu-zeolites catalyst under the SO₂ exposure and absence of NH₃. It was reported that at different temperatures, the poisoning of catalyst is different. The SO₂ exposure of unspecified Cu-zeolite has been reported high deactivation of catalyst at 200 °C as compared with 300 °C. Overall least deactivation has been found at 400 °C after the exposure of SO₂ [58]. Cu/SSZ-13 also showed the same trend as above [22], catalyst was more deactivated at 250 °C as compared to 400 °C after poisoning. But the Cu/SAPO-34 showed the opposite trend than the Cu/SSZ-13, it has been reported that Cu/SAPO-34 was more deactivated at 250 °C than the 150 °C after sulfation [59]. Also it has been shown that the Cu/SAPO-34 was more deactivated at 400 °C as compared to 200 °C after the SO₂ exposure [57].

4.5.3. SO₂ + NH₃ impact on SCR catalyst activity

A comparative study between sulfation and with or without the presence of ammonia reported that, with the presence of NH₃ at the temperature of 300 °C after sulfation, more deactivation of catalyst was found [56]. Also, the same trend has been shown in another study [57], at temperature 400 °C during the presence of NH₃, poisoning of SO_x produced the more negative affect as compared to the poisoning of SO_x without the use of NH₃.

4.5.4. SO₂ and/or SO₃ impact on SCR catalyst activity

SO₃ poisoning has produced more significant impact of deactivation as compared with SO₂ poisoning. Unspecified Cu-zeolites was used to investigate the impact of poisoning temperature. With the increase of poisoning temperature (200, 300, 400 °C) more deactivation has been reported [60]. Also, at the same temperature conditions, the impact of SO₂ as compared with SO₃ was investigated. It has been reported that poisoning of SO₃ resulted more significant deactivation than the SO₂ poisoning for all temperature ranges.

During the investigation of Cu/SAPO-34 catalyst it has been observed that for SO_3 poisoning temperature was an important parameter [61]. Poisoning of SO_2 and $\text{SO}_2 + \text{SO}_3$ at temperature of 200 °C both has same impact on the catalyst activity. However, $\text{SO}_2 + \text{SO}_3$ poisoning at temperature of 400 °C was responsible for the severe deactivation of catalyst than the SO_2 poisoning. It has been reported that the mechanism for the poisoning of SO_2 and SO_3 was different, whereas poisoning of SO_2 is due to the adsorption and poisoning of SO_3 is because of chemical reactions having activated temperature with catalyst surface.

Cu-zeolite catalyst associated with poisoning of sulfur was studied by putting 35 ppm of SO_2 in a “diesel system simulator” (DSS). It consists of diesel oxidation catalyst (DOC) at the upstream of catalyst soot filter (CSF) and followed by SCR system. Since the SCR reactor was located after the DOC, therefore some part of SO_2 oxidized into SO_3 . It has been proved that after the 400 hours the activity of SCR reactor started to lose, which was about 4g of sulfur/litre [62].

4.5.5. Sulfur storage on Cu-zeolites

Many papers have been reported the storage of sulfur on Cu-zeolite and the poisoning of SO_2 . It has been observed that different temperatures have different impact on sulfur storage. A Cu/SAPO-34 [59] and unspecified Cu-chabazite [57] catalysts with chabazite structure were studied by considering the sulfur storage on catalysts. It has been reported in both investigations that exposure of SO_2 at high temperatures first at (350 °C vs 190 °C) and later at (250 °C vs 150 °C) showed sulfur storage in large amount. In another study [58] unspecified Cu-zeolite showed the opposite trend, where exposure of SO_3 at low sulfation temperature (Setting temperature for results: 200 °C, 300 °C and 400 °C) reported large amount of sulfur storage. However, it has also been investigated in same study; the catalyst activity showed the larger decline at high temperatures after the sulfation.

It was investigated that sulfur storage impacted with the different forms of sulfur [57, 58] both reported that the sulfur storage as a result of SO_3 exposure is more than SO_2 exposure. Also, it has been observed that during sulfation period, the sulfur storage at the present of NH_3 is more affected than the absence of NH_3 [56, 59, 63].

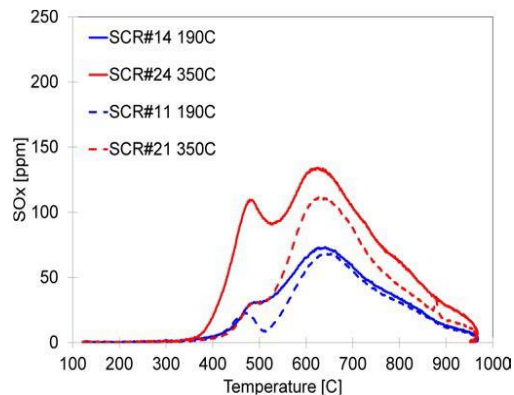


Fig.5. SO_x released during TPD on four different sulfur saturated chabazite structure SCR catalysts. Sulfur saturation of SO_2 and SO_3 was shown by solid lines and only SO_2 by dotted lines. At the temperature of 190 °C and 350 °C, blue and red lines were sulfur saturated respectively

Temperature programmed desorption (TPD) was used to investigate the sulfur storage on the four different sulfur saturated chabazite structure SCR catalysts. Fig. 5 showed the TPD diagram. Sulfur saturation of SO_2 and SO_3 was shown by solid lines and only SO_2 by dotted lines. At the temperature of 190 °C and 350 °C, blue and red lines were sulfur saturated respectively. At DOC, SO_2 was oxidized into SO_3 , therefore the ratio of SO_3 and SO_2 largely depends upon the sulfation temperature. At high sulfation temperatures, significant amount of SO_3 can be estimated. Two peaks have been shown in all TPD curves first at ca 480 °C and second at ca 650 °C. It has been concluded that for both SO_3 and SO_2 , sulfur storage was much more after sulfation as compared to only SO_2 . Furthermore, at high temperature (350 °C), more sulfur storage occurs after sulfation than the low temperature (190 °C) [57].

4.5.6. Regeneration of sulfated cu-zeolite

It has been reported that different type of ways showed different results while regenerating the sulfated Cu-zeolites. Sulfation of 200 ppm of SO₂ at 130 °C for 3 hours was carried out to regenerate the Cu/SAPO-34 catalyst [46]. Regeneration of a Cu/SAPO-34 catalyst was performed for 12 hours by varying temperatures at 300, 400, 500, 600 and 700 °C. Up to temperature of 600 °C, regenerated catalyst showed the limited recovery in NO removal efficiency. The regeneration of catalyst was fully observed at 600 °C.

Various sulfation methods were used to investigate the regeneration of Cu-chabazite catalyst [57]. It has been observed that the regeneration of SO₂ aged catalyst at low temperature (200 °C) was easier than the high temperature (400 °C) aged. Furthermore, during the comparison of SO₂ aged catalyst, with and without the presence of NH₃, no difference has been observed in the regeneration of catalyst. A repeated activity test has been performed for the regeneration of Cu/SSZ-13 catalyst at temperatures in between of 100 °C to 400 °C [56]. Catalyst with exposure of SO₂ poisoning (30 ppm) was investigated at temperature of 300 °C for 1.5 hours. Eight activity tests have been performed to obtain the stable activity. It has been observed from the experiment that by repeating the activity test some activity was recovered but not achieving the fully regeneration of catalyst.

Cu-chabazite catalyst was used to investigate the regeneration also named as chemical deSO_x method [21]. For reducing the environmental problems, low concentration of reductant such as NH₃, NO_x+NH₃, C₂H₆ and n-C₁₂H₂₆ was used. By using this technique, it has been observed that at lower regeneration temperatures, recovery of NO_x conversion activity and removal of sulfur was achieved.

4.5.7. Characterizations of sulfated cu-zeolites

Sulfated catalyst has been characterized in many studies. N₂ adsorption is used to determine to surface area and its pore volume. It has been observed that after the sulfation both surface area and pore volume were decreased [20-22, 56]. But after regeneration both could be recovered [22]. X-ray fluorescence (XRF) was used to investigate the framework of SAPO-34 and it has been observed that it was not changed after the poisoning of SO₂. This recommends that sulfur only affects the copper sites of catalyst not the framework of zeolite [64].

Analysis of Inductively coupled plasma (ICP) and X-ray photoelectron spectroscopy (XPS) were used to investigate the sulfur distribution, it has been found that, sulfur was uniformly distributed only if the catalyst was saturated [57, 61]. More sulfur has been observed at the catalyst inlet as compared to outlet, if the catalyst was not saturated properly [56, 58].

Numerous methods have been reported to determine the type in which storage of sulfur is taken place over the sulfated Cu-zeolite. It has been observed that there are two primary sulfur species such as ammonium sulfates and copper sulfates depending upon the sulfation conditions [46, 58, 59]. Formation of ammonium and copper sulfates was studied on the Cu/SAPO-34 catalyst [65]. It has been observed that ammonium and copper sulfates are exchangeable depends upon the availability of NH₃. Ammonium sulfates can be formed by NH₃ exposure of copper sulfates over the catalyst. During the absence of NH₃ the usage of ammonium sulfates upon the NO exposure behaves as SCR reactant. However, this reaction is much slow as compared to normal SCR reaction. Also, copper sulfates are formed when the SCR reactants are ammonium sulfates.

4.5.8. Sulfur poisoning mechanism on copper zeolite

Cu/SSZ-13 catalyst was used to investigate the active sites. Diffuse reflectance infrared Fourier transform spectroscopy (DRIFTS) with NH₃ probing was used to identify the two cu-sites. In SCR reactions both sites were active but in oxidation reactions only one site was active. Furthermore, also their responses towards sulfur poisoning and hydrothermal aging were investigated. In oxidation reaction the active site was disappeared and in SCR reaction, both active site was reduced extensively [66]. After SO₂ poisoning, the activity loss over the Cu/SAPO-34 catalyst was described by the reduction in the active sites of Cu-zeolite because of the sulfur present in the catalyst. It has been observed that the NO conversion and sulfur exposure showed inverse relationship if sulfur exposure was increased then NO conversion was decreased [64].

4.6. Behavior of sulfur over SCR catalysts with different temperatures (Recent developments)

SO₂ poisoning of NH₃-SCR was evaluated by Yasser [67] over Cu-SAPO-34, mainly to investigate stored S forms/states and the effect of them on reduction activity of low-temperature NOx. There were two types of primary sulfur species found, and it was observed that they both were interchangeable depending upon the availability or the absence of NH₃. Cu sulfate species as well as Ammonium sulfate species could be found in one case, while for the other case only Cu sulfate species would be found. Cu sulfate was available in three different states/forms when ammonia was absent, this was found out by three desorption features while conducting experiments of TPD (temperature programmed desorption). NO adsorption's DRIFTS (Diffuse reflectance infrared Fourier transform spectroscopy) was utilized for the investigation of accessibility and nature of

Cu species prior to and after the sulfate formation, subject to no intrusion by ammonium sulfate; the acquired states showed that the sulfur had completely blocked Cu²⁺ within the six membered rings, and nature of [CuOH]⁺ near the eight-membered ring had changed. On analyzing impacts of dissimilar states of S on reduction activity of NO_x, ammonium sulfate having low-temperature was found to have the greatest effect on the loss of performance. Moreover, the data demonstrated that ammonium sulfate have tendency to work as SCR reactant, quite similar to the system incorporating ammonium nitrate. Decomposition of Ammonium sulfate starts at temperatures which can be as small as 300–350 °C, in contrast to that higher temperatures (>480 °C) were required for desorption of other S containing species as illustrated in fig 6.

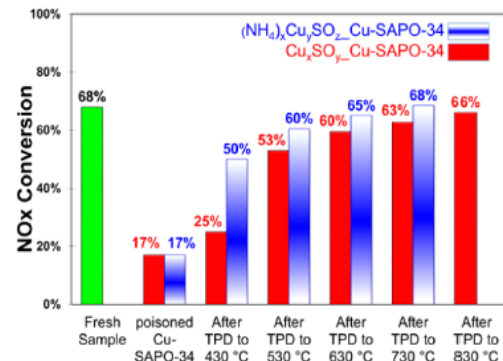


Fig. 6. SCR changing at 210 °C along with the raw sample, during existence of SO₂ quantity 50 ppm, sample on which Cu_xSO_y was materialized and later brought to temperatures of 430, 530, 630, 730, and 830 °C in presence of (NH₄)_x or N₂

This seems promising, as reaction of NH₃ can occur in the presence of catalyst with reabsorbed sulfur to form ammonium sulfate, having tendency to decompose at smaller temperatures as compared to other forms of sulfate.

Sandra [68] observed the impacts of Sulphur experimentally, upon low-temperature behavior of Cu-SSZ-13 SCR catalyst. The outcomes of exposure

temperature of sulfur, and impacts of NO_x/NO_2 ratio, are taken into consideration and a comparison of two separate regeneration temperatures is performed. Besides that, samples of catalyst taken from catalyst affected by an engine-aged are analyzed. Exposition temperature of SO_2 possesses important effect on Cu-SSZ-13 catalyst deactivation. The most severe deactivation is caused due to lowest Sulphur exposure temperature (220°C), whereas during the highest temperature of Sulphur exposure (400°C) deactivation of the lowest degree is observed as demonstrated in figure 7.

Yulong [69] investigated the hydrothermal aging at prominent temperature. Not the same as the reversible hindrance of SO_2 harming that happens at truncated temperatures, because of the demolition of the zeolite structure the sulfur harming at prominent temperature is long-lasting.

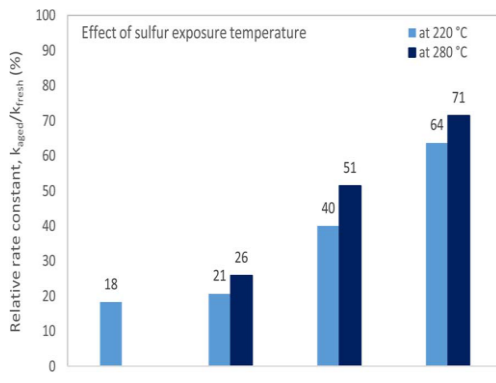


Fig. 7. Relative rate constants for catalyst exposed at different temperature ranges. Note that, the sample which was brought at 220°C to SO_2 had no test at 280°C . 5 vol.-% H_2O , 10 vol.-% O_2 1000 vol.-ppm NH_3 , 1000 vol.-ppm NO , $120,000 \text{ h}^{-1}$ GHSV during the test of activity.

In Figure 8 the benchmark SCR NO_x and NH_3 transformation exercises of HA-Cu-SSZ-13, FR-Cu-SSZ-13 and SA-Cu-SSZ-13 chemical agents are portrayed by means of a portion of temperature as of 150 to 550°C . It has been observed the new Cu-SSZ-13 showed the finest NH_3 -SCR action on entire temperature ranges. The decrease action of

NO weakened somewhat for the Cu-SSZ-13 afterwards it was hydrothermally aged at 750°C aimed at 32h. For the SA-Cu-SSZ-13 test critical loss of not any decreased movement was watched that was hydrothermally aged within the sight of 100 ppm SO_2 . Throughout hydrothermal aging proposed deactivation of Cu-SSZ-13 was significantly more extreme within the sight of SO_2 . The NH_3 change is a lot advanced than any transformation due to unselective NH_3 oxidation. When the temperatures over 450°C and 300°C aimed at the SA-Cu-SSZ-13 and HA-Cu-SSZ-13 tests, the uncritical NH_3 oxidation was fundamentally in charge for the decomposition of not any adaptation at prominent temperatures.

Meiqing [70] investigated the impact of SO_3 poisoning over Cu/SAPO-34.

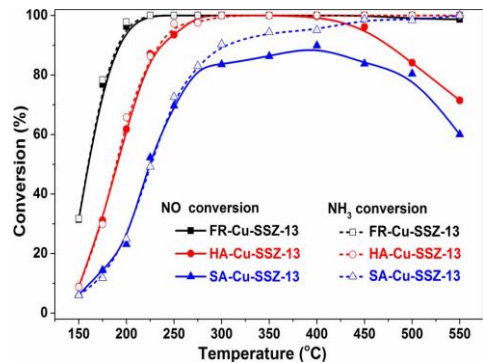


Fig. 8. NO and NH_3 = 500 ppm, 5 vol.-% O_2 , 5 vol.-% H_2O , equilibrium N_2 . $\text{GHSV} = 400,000 \text{ h}^{-1}$. NO_x and NH_3 change of HA-Cu-SSZ-13, FR-Cu-SSZ-13 and SA-Cu-SSZ-13 catalysts below normal SCR circumstances.

Fig. 9 The reaction of NH_3 SCR consisting sulfated and fresh Cu/SAPO-34 catalysts is shown. In comparison to F-Cu, declines in NO_x conversion are seen of sulfated catalysts when SO_3 to SO_x ratio increases. Remarkably, throughout the whole temperature region, S-20-Cu was found to be least active catalyst of all kinds of sulfated samples. Unsulfured catalysts having 600 C (7 ppm) has the highest N_2O formation on it, and the sulfation action results in reduction of the formation of N_2O by 1 to 2 ppm. (Fig. 8b).

In this work [71] the deactivation conducts and procedure of a Cu-SAPO-34 catalyst by reactor trial and DFT computations was studied. The dignified steady state of NO_x changes for the new catalyst can be determined from the figure 1A, after introduction to SO₂, and subsequently regeneration at 550 °C. After introduction of SO₂, 1.5 ppm portion was added to the SCR-feed, SO₂ concentration is also presumed in automotive diesel exhaust, for 8h we detained the new catalyst at 300 °C, Execution at 550 °C for 1 h in SCR-feed gas in the absence of SO₂ for renewal of the catalyst. When SO₂ was introduced it resulted in significantly lesser steady state NO_x changes in the temperature variety 150–300 °C.

For all intents and practical purposes after probing SO₂ deactivation, it is frequently convenient towards quicken the SO₂-harming by rising the concentration of SO₂ and

proportionally abbreviating the exposure period. The outcomes are then construed in appellation of the overall SO₂ exposure, considered as the formation of the SO₂ fractional pressure and the exposure period, instead of the SO₂ concentration. This elucidation needs that a straight proportionality occurs and the exposure period and SO₂ concentration, in a way that dual framework can be climbed with respect to SO₂-harming. By estimating the outcomes of the non-accelerated SO₂ introduction scalability was scrutinized for example introduction to 1.5 ppm SO₂, towards the outcomes from a catalyst revealed to an enhanced SO₂ introduction. Meant for the enhanced SO₂ introduction, the concentration of SO₂ was enlarged by a number 10 and the introduction time was harmoniously reduced.

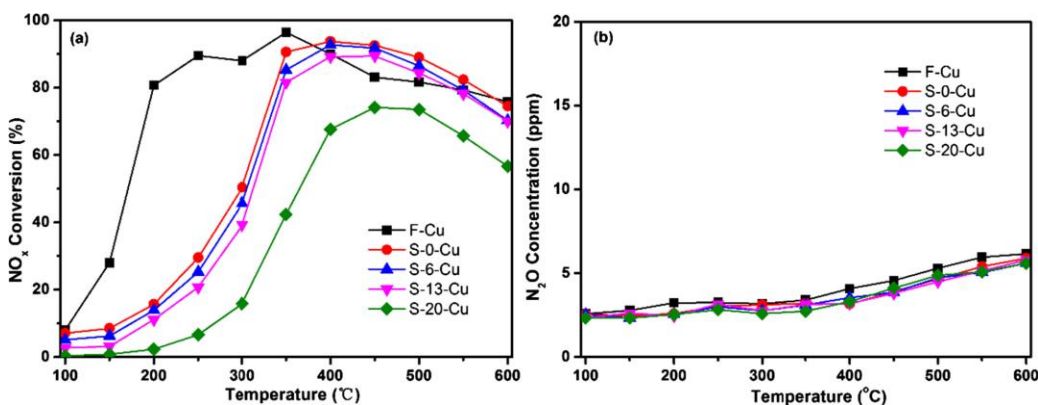


Fig. 9. NO_x conversion as a relation pertaining to reaction temperature on the raw and sulfated catalysts S-0-Cu = 50 ppm of SO₂ for 16h, S-6-Cu = 50 ppm of SO_x (6% SO₃) for 16h, S-13-Cu = 50 ppm of SO_x (13% SO₃) for 16h and S-20-Cu 50 ppm of SO_x (20% SO₃) for 16h (a) and emergence of N₂O in course of NH₃ SCR reaction over the fresh and sulfated catalysts (b)The execution of reaction was done with a mixture containing NO_x 500 ppm, NH₃ 500 ppm, 7% CO₂, 5% O₂, 3% H₂O, and balance N₂ owing to GHSV = 72,000 h⁻¹

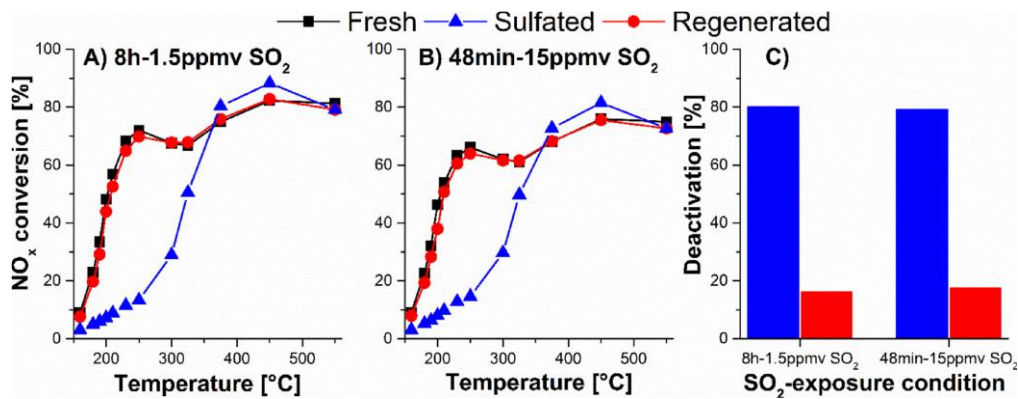


Fig. 10(A) NO_x as purpose of temperature exhibits its conversion for the Cu-SAPO-34 catalyst earlier and later experience to 1.5 ppm (B) The temperature for the Cu-SAPO-34 by NO_x conversion catalyst earlier and later exposure to 15 ppm (C) After deactivation the sulfated (blue inns) and recovered (red inns) express the Cu-SAPO-34 catalysts assessed at 180 °C, afterwards introduction to 1.5 ppm SO₂ aimed at 8h and 15 ppm SO₂ aimed at 48 min.

Therefore, in the SO₂ in SCR-feed gas was exposed to 15 ppm for 48 min at 300 °C. Figure 10B illustrates the stable state of NO_x changes earlier and later the accelerated SO₂ exposure, and later 1 h renewal at 550 °C inside SCR-feed gas. The outward form of the NO_x changes is for the enhanced SO₂ introduced catalyst in Fig. 10B, it is very analogous to the revealed inside figure 10A, figure 10B.

Illustrates the NO_x vicissitudes of the new catalyst is somewhat underneath those of the new catalyst in figure 10A which is because of slight variances in the catalyst loads. Hence, to check the resemblance of the impact of the enhanced and non-enhanced SO₂ exposure circumstances on the SCR presentation of the catalyst, the deactivation (assessed at 180 °C) after SO₂ experience and renewal are illustrated in Figure 10C. After both behaviors the degree of deactivation is similar with overall deactivations of 80 and 79% and permanent deactivations of 16% and 18%. For the same total exposure, it signifies that the deactivation is identical, here SO₂ concentration and revelation period are scalable.

5. Summary

Vanadium based catalysts can be impacted by sulfur exposure in different ways. If NH₃ is absence during poisoning at high temperatures, NO_x activity can be increased. If NH₃ is present during the sulfur exposure of catalyst, formation of ammonium sulfates can be produced, which ultimately results the physical deactivation of catalyst. The decomposition of ammonium sulfates occurs when the temperature in between 280-350 °C and also by increasing the temperature regeneration of catalyst can be achieved. Consequently, the main problem occurs with vanadium-based catalyst when the high level of sulfur is exposed at low temperatures. Thus, the catalyst temperature never exceeds the decomposition temperature.

NO_x activity can be deactivated with sulfur exposure of Cu-zeolites catalysts. SO₃ poisoning is capable to produce severe deactivation of catalyst activity, high sulfur storage and very hard to regenerate the catalyst as compared to SO₂ poisoning. SO₃ and SO₂ poisoning are not reliable with impact of temperature. It has been recommended that, at high temperature chemisorption occurs over the catalyst surface and at low temperature formation of ammonium sulfate and physical adsorption

occurs. Two sulfated species were observed while characterizing the sulfated Cu-zeolite named as ammonium and copper sulfates. It has been recommended that sulfated species is the main cause of deactivation which ultimately blocks the active Cu-sites, either by the formation of ammonium and copper sulfates that blocks the active sites of catalyst physically or by adsorption of sulfur species. Furthermore, sulfur poisoning does not affect the zeolite structure, but it only affects the active sites of copper. Sulfated catalysts have been regenerated in a lean environment by increasing exposure temperature about to 600-700 °C.

ACKNOWLEDGEMENT

I would like to thank the National Key R&D Program of China (2016YFC0205200) and the Ministry of Industry and Information Technology of Marine Low-Speed Engine Project Phase – I for supporting this work.

REFERENCES

- [1] P. Geng, "Effects of alternative fuels on the combustion characteristics and emission products from diesel engines," *A review. Renewable and Sustainable Energy Reviews*, Vol. 71, 2017, pp. 523-534.
- [2] N. Hu, P. Zhou, and J. Yang, "Reducing emissions by optimising the fuel injector match with the combustion chamber geometry for a marine medium-speed diesel engine," *Transportation Research Part D: Transport and Environment*, Vol. 53, 2017, pp. 1-16.
- [3] C. Zhang, C. Suna, M. Wua, and K. Lub, "Optimization design of SCR mixer for improving deposit performance at low temperatures," *Fuel* Vol. 237, 2019, pp. 465-474.
- [4] W. Chen, H. Fali, L. Qin, H. Jun, B. Zhao, T. Yangzhe, and Y. Fei, "Mechanism and Performance of the SCR of NO with NH₃ over Sulfated Sintered Ore Catalyst." *Catalysts* Vol. 9, 2019, pp. 90-101.
- [5] C. Baukal, "Everything you need to know about NOx: Controlling and minimizing pollutant emissions is critical for meeting air quality regulations," *Metal finishing*, Vol. 103, 2005, pp. 18-24.
- [6] Gu, "A potentially over estimated compliance method for the Emission control Areas," [7] *Transportation Research Part D*, Vol. 55, 2017, pp. 51-66.
- [8] A. Aberg, A. Widd, J. Abildskov, and J.K. Huusom, "Parameter estimation and analysis of an automotive heavy-duty scr catalyst model," *Chemical Engineering Science*, Vol. 161, 2017, pp. 167-177.
- [9] E. Codan, S. Bernasconi, and H. Born, Imo III emission regulation: Impact on the turbocharging system, *CIMAC Congress*, 2010.
- [10] R. Geertsma, R. Negenborn, K. Visser, M. Loonstijn, and J. Hopman, "Pitch control for ships with diesel mechanical and hybrid propulsion: Modeling, validation and performance quantification," *Applied Energy*, Vol. 206, 2017, pp. 1609-1631.
- [11] L. XR, "Combustion and emission characteristics of a lateral swirlcombustion system for DI diesel engines under low excess air ratio conditions," *Fuel*, Vol. 186, 2016, pp. 672-80.
- [12] C. K, P. J, and K. SL, "A comparison of Reactivity Controlled Compression Ignition (RCCI) and Gasoline Compression Ignition (GCI) strategies at high load, low speed conditions," *Energy Convers Manag*, Vol. 127, 2016, pp. 324-41.
- [13] A. Güthenke, D. Chatterjee, M. Weibel, M. Krutzsch, B. Kocí, P. Marek, M. Nova, and E. Tronconi, "Current status of modeling lean exhaust gas aftertreatment catalysts", *Advances in Chemical Engineering*, Vol. 33(07), 2007.
- [14] M. Koebel, M. Elsener, and M. Kleemann, "Urea-SCR: A promising technique to reduce NOx emissions from automotive diesel engines," *Catalysis Today*, Vol. 59(3/4), 2000, pp. 335-345.
- [15] Oliveira, "Modeling of NOx emission factors from heavy and light-duty vehicles equipped with advanced after treatment systems," *Energy Conversion and Management*, Vol. 52, 2011, pp. 2945-2951.
- [16] S.S. P, "A Review on Selective Catalytic Reduction (SCR)-A Promising Technology to mitigate NOx of Modern Automobiles," *International Journal of Applied Engineering Research*, Vol. 13, 2018, pp. 5-9.
- [17] F. Birkhold, "Modeling and simulation of the injection of urea-water solution for automotive Scr deNox-systems," *Applied Catalysis B: Environmental*, Vol. 170, 2007, pp. 119-127.
- [18] C. Choi, "Numerical Analysis of Urea Decomposition with Static Mixers in Marine SCR System," *Journal of Clean Energy Technologies*, Vol. 3(1), 2015, pp. 39-42.

- [18] Y. Xi, N. A. Ottinger and G. Liu, "New insights into sulfur poisoning on a vanadia SCR catalyst under simulated diesel engine operating conditions," *Applied Catalysis B: Environmental*, Vol. 64, 2014, pp. 1-9.
- [19] I. Nova and E. Tronconi, "Urea-SCR Technology for deNOx After Treatment of Diesel Exhausts," *Springer*, 2014.
- [20] B. K. Yun, and M.Y. Kim, "Modeling the selective catalytic reduction of NOx by ammonia over a vanadium-based catalyst from heavy duty diesel exhaust gases," *Applied Thermal Engineering*, Vol. 50, 2013, pp. 152-158.
- [21] H. L. Fang, H.F.M, and DaCosta, "Urea thermolysis and NOx reduction with and without SCR catalysts." *Appl. Catal. B: Environ*, Vol. 46, 2013, pp. 14-34.
- [22] X. Liu, X. Wu, D. Weng and Z. Si, "Durability of Cu/SAPO-34 catalyst for NOx reduction by ammonia: Potassium and sulfur poisoning," *Catalysis Communications*, Vol. 59, 2014, pp. 35-39.
- [23] A. Kumar, M. A. Smith, K. Kamasamudram, N. W. Currier and Y. Aleksey, "Chemical deSOx: An effective way to recover Cu-zeolite SCR catalysts from sulfur poisoning," *Catalysis Today*, Vol. 267, 2016, pp. 10-16.
- [24] D. W. Brookshear, J.-g. Nam, K. Nguyen, T. J. Toops and A. Binder, "Impact of sulfation and desulfation on NOx reduction using Cu-chabazite SCR catalysts," *Catalysis Today*, Vol. 258, 2015, pp. 359-366.
- [25] D. Chatterjee and K. Rusch, "Urea-SCR Technology for deNOx After Treatment of Diesel Exhausts," *Springer*, 2014.
- [26] J. Wang, H. Zhao, G. Haller and Y. Li, "Recent advances in the selective catalytic reduction of NOx with NH₃ on Cu-Chabazite catalysts," *Applied Catalysis B: Environmental*, Vol. 202, 2017, pp. 346-354.
- [27] K. Leistrner, O. Mihai, K. Wijayanti, A. Kumar, K. Kamasamudram, N. W. Currier, A. Yezerets and L. Olsson, "Comparison of Cu/BEA, Cu/SSZ-13 and Cu/SAPO-34 for ammonia-SCR reactions," *Catalysis Today*, Vol. 258, 2015, pp. 49-55.
- [28] Y. Peng, et al., "Comparison of MoO₃ and WO₃ on arsenic poisoning V₂O₅/TiO₂ catalyst: DRIFTS and DFT study," *Applied Catalysis. B*, Vol. 181, 2016, pp. 692-698.
- [29] S. M. Lee, K.H. Park, and S.C. Hong, MnOx/CeO₂-TiO₂ mixed oxide catalysts for the selective catalytic reduction of NO with NH₃ at low temperature," *Chemical Engineering Journal*, Vol. 13, 2012, pp. 323-331.
- [30] Y. Qiu, et al., "The monolithic cordierite supported V₂O₅-MoO₃/TiO₂catalyst for NH₃-SCR," *Chemical Engineering Journal*, Vol. 294, 2016, pp. 264-272.
- [31] M. Shimokawabe, "SCR of NO by DME over Al₂O₃ based catalysts: Influence of noble metals and Ba additive on low-temperature activity," *Catalysis Today*, Vol. 164, pp. 480-483.
- [32] S. S. Kim, "Enhanced catalytic activity of Pt/Al₂O₃ on the CH₄ SCR," *Journal of Industrial and Engineering Chemistry*, Vol. 18, 2012, pp. 272-276.
- [33] L.M. Yu, et al., "Enhanced NO_x removal performance of amorphous Ce-Ti catalyst by hydrogen pretreatment. Journal of Molecular," *Catalysis A*, Vol. 423, 2016, pp. 371-378.
- [34] X. Liu, et al., "Probing NH₃-SCR catalytic activity and SO₂ resistance over aqueous-phase synthesized Ce-W@TiO₂ catalyst," *Journal of Fuel Chemistry and Technology*, Vol. 44, 2016, pp. 225-231.
- [35] C. K. Seo, et al., "Effect of ZrO₂ addition on de-NO_x performance of Cu-ZSM-5 for SCR catalyst," *Chemical Engineering Journal*, Vol. 191, 2012, pp. 331-340.
- [36] P. NakhostinPanahi, "Comparative study of ZSM - 5 supported transition metal (Cu, Mn, Co, and Fe) nanocatalysts in the selective catalytic reduction of NO with NH₃," *Environmental Progress and Sustainable Energy*, Vol. 36, 2017, pp. 1049-1055.
- [37] X. L. Tang, et al., "Low-temperature SCR of NO with NH₃ over AC/C supported manganese-based monolithic catalysts," *Catalysis Today*, Vol. 126, 2007, pp. 406-411.
- [38] B. C. Huang, et al., "Low temperature SCR of NO with NH₃ over carbon nanotubes supported vanadium oxides," *Catalysis Today*, Vol. 126, 2007, pp. 279-283.
- [39] C. H. Bartholomew, "Mechanisms of catalyst deactivation," *Applied Catalysis A: General*, Vol. 212, 2001. pp. 17- 60.
- [40] M. V. Twigg, "Progress and future challenges in controlling automotive exhaust gas emissions," *Applied Catalysis B: Environmental*, Vol. 70, 2007, pp. 2-15.
- [41] A. Varna, A.C. Spiteri, and Y.M. Wright, "Experimental and numerical assessment of impingement and mixing of urea-water sprays for nitric oxide reduction in diesel exhaust," *Applied Energy*, Vol. 157, 2015, pp. 824-837.
- [42] S. Grout, J.B. Blaisot, and K. Pajot, "Experimental investigation on the injection of an urea-watersolution in hot air stream for the SCR application: Evaporation and spray/wall interaction," *Fuel*, Vol. 106, 2013, pp. 166-177.

- [43] MAN B&W. MAN emission project guide: MAN B&W two-stroke marine engines. EU: MAN B&W press 2013.
- [44] R. M. Heck, R. J. Farrauto and S. T. Gulati, Catalytic air pollution control Commercial Technology, 3ed., New Jersey: John Wiley & Sons, Inc., 2009.
- [45] Y. H. Shi, H. Shu, Y.-H. Zhang, H.-M. Fan, Y.-P. Zhang and L.-J. Yang, "Formation and decomposition of NH₄HSO₄ during selective catalytic reduction of NO with NH₃ over V₂O₅-WO₃/TiO₂ catalysts," *Fuel Processing Technology*, Vol. 150, 2016, pp. 141-147.
- [46] L. Zhang, D. Wang, Y. Liu, K. Kamasamudram, J. Li and W. Epling, "SO₂ poisoning impact on the NH₃-SCR reaction over a commercial Cu-SAPO-34 SCR catalyst," *Applied Catalysis B: Environmental*, Vol. 157, 2014, pp. 371-377.
- [47] R. Q. Long, R. T. Yang and R. Chang, "Low temperature selective catalytic reduction (SCR) of NO with NH₃ over Fe-Mn based catalysts," *Chem. Communication*, Vol. 5, 2012, pp. 452-453.
- [48] W. T. Mu, J. Zhu, S. Zhang, Y. Y. Guo, L. Q. Su, X. Y. Li and Z. Li, "Styrene hydrogenation performance of Pt nanoparticles with controlled size prepared by atomic layer deposition," *Catal. Sci. Technol.*, Vol. 6, 2016, pp. 7532-7548.
- [49] C. U. I. Odenbrand, "Urea-SCR Technology for deNOx After Treatment of Diesel Exhausts," *Chem. Eng. Res. Des.*, Vol. 86, 2008, pp. 663-672.
- [50] J. P. Chen, M. A. Buzanowski, R. T. Yang and J. E. Cichanowicz, "Deactivation of the Vanadia Catalyst in the Selective Catalytic Reduction," *Process Air Waste Manage*, Vol. 40, 1990, pp. 1403-1409.
- [51] X. Y. Guo, [MS Dissertation], Brigham Young University, 2006, pp. 25-28.
- [52] L. Chmielarz, R. Dziembaj, T. Łojewski, A. Węgrzyn, T. Grzybek, J. Klinik and D. Olszewska, "Deactivation of SCR Catalysts by Exposure to Aerosol Particles of Potassium and Zinc Salts," *Solid State Ionics*, Vol. 141, 2001, pp. 715-719.
- [53] C. Orsenigo, A. Beretta, P. Forzatti, J. Svachula, E. Tronconi, F. Bregani and A. Baldacci, "Theoretical and experimental study of the interaction between NO_x reduction and SO₂ oxidation over DeNO_x-SCR catalysts," *Catal. Today*, Vol. 27, 1996, pp. 15-21.
- [54] P. D. Ji, X. Gao, X. S. Du, C. H. Zheng, Z. Y. Luo and K. F. Cen, "Relationship between the molecular structure of V₂O₅/TiO₂ catalysts and the reactivity of SO₂ oxidation," *Catal. Sci. Technol.*, Vol. 6, 2015, pp. 1187-1194.
- [55] G. Busca, L. Lietti, G. Ramis and F. Berti, "Characterization and Reactivity of V₂O₅-MoO₃/TiO₂ De-NO_x SCR Catalysts," *Appl. Catal. B*, Vol. 18, 1998, pp. 1-36.
- [56] K. Wijayanti, K. Leistner, S. Chand, A. Kumar, K. Kamasamudram, N. W. Currier, A. Yezerets and L. Olsson, "Deactivation of Cu-SSZ-13 by SO₂ exposure under SCR conditions," *Catalysis Science & Technology*, Vol. 6, 2016, pp. 2565-2579.
- [57] A. Kumar, J. Li, J. Luo, S. Joshi, A. Yezerets and K. Kamasamudram, "Catalyst Sulfur Poisoning and Recovery Behaviours: Key for Designing Advanced Emission Control Systems," *SAE International*, 2017.
- [58] Y. Cheng, C. Lamberg, D. H. Kim, J. H. Kwak, S. J. Cho and C. H. Peden, "The different impacts of SO₂ and SO₃ on Cu/zeolite SCR catalysts," *Catalysis Today*, Vol. 151, 2010, pp. 266-270.
- [59] C. Wang, J. Wang, J. Wang, T. Yu, M. Shen, W. Wang and W. Li, "The effect of sulfate species on the activity of NH₃-SCR over Cu/SAPO-34," *Applied Catalysis B: Environmental*, Vol. 204, 2017, pp. 239-249.
- [60] Y. Cheng, C. Montreuil, G. Cavataio and C. Lambert, "The Effects of SO₂ and SO₃ Poisoning on Cu/Zeolite SCR Catalysts," *SAE International*, Dearborn, USA, 2009.
- [61] A. Kumar, M. A. Smith, K. Kamasamudram, N. W. Currier, H. An and A. Yezerets, "Impact of different forms of feed sulfur on small-pore Cu-zeolite SCR catalyst," *Catalysis Today*, Vol. 231, 2014, pp. 75-82.
- [62] W. Tang, X. Huang and S. Kumar, "Department of Energy," 04 October 2011. [Online]. Available: https://energy.gov/sites/production/files/2014/03/f8/deer11_tang.pdf. [Accessed April 3 2017].
- [63] Y. Jangjou, D. Wang, Kumar, Ashok, J. Li and W. S. Epling, "SO₂ Poisoning of the NH₃-SCR Reaction over Cu-SAPO-34: Effect of Ammonium Sulfate versus Other S-Containing Species," *ASC Catalysis*, Vol. 6, 2016, pp. 6612-6622.
- [64] M. Shen, H. Wen, T. Hao, T. Yu, D. Fan, J. Wang, W. Li and J. Wang, "Deactivation mechanism of SO₂ on Cu/SAPO-34 NH₃-SCR catalysts: structure and active Cu²⁺," *Catalysis Science & Technology*, Vol. 5, 2015, pp. 1741-1749.
- [65] Y. Jangjou, D. Wang, A. Kumar, J. Li and W. S. Epling, "SO₃ Positioning of the NH₃-SCR Reaction over Cu-SAPO-34," *ACS Catalysis*, Vol. 6, 2016, pp. 6716-6728.
- [66] J. Luo, D. Wang, A. Kumar, J. Li, K. Kamasamudram, N. Currier and A. Yezerets,

- [66] “Identification of two types of Cu sites in Cu/SSZ-13 and their unique responses to hydrothermal aging and sulfur poisoning,” *Catalysis Today*, Vol. 267, 2016, pp. 3-9.
- [67] Y. Jangjou, D. Wang, A. Kumar, J. Li, and S. William, “SO₂ Poisoning of the NH₃-SCR Reaction over Cu-SAPO-34: Effect of Ammonium Sulfate versus Other S containing Species,” *ACS Catal.*, 6, 2016, pp. 6612–6622.
- [68] S. Dahlma, C. Lanttob, J. Englund, B. Westerbergd, F. Regalid, M. Skoglundhc, L. J. Pettersson, “Chemical aging of Cu-SSZ-13 SCR catalysts for heavy-duty vehicles – Influence of sulfur dioxide,” *Catalysis Today* 320, 2019, pp. 72–83.
- [69] Y. Shan, X. Shi, Z. Yan, J. Liu, Y. Yu, H. He, “Deactivation of Cu-SSZ-13 in the presence of SO₂ during hydrothermal aging,” *Catalysis Today*, 320, 2019, pp. 84–90.
- [70] M. Shen, Y. Zhang, J. Wang, C. Wang, J. Wang, “Nature of SO₃ poisoning on Cu/SAPO-34 SCR catalysts,” *Journal of Catalysis*, 358, 2018, pp. 277–286.
- [71] P. S. Hammershoi, P. N.R. Vennestrom, H. Falsig, A. D. Jensen, T. V.W. Janssens, “Importance of the Cu oxidation state for the SO₂-poisoning of a Cu-SAPO-34 catalyst in the NH₃-SCR reaction,” *Applied Catalysis B: Environmental.* 236, 2018, pp. 377–383.

Stabilization of Non-holonomic 03 DOF Hovercraft using Robust RST Control Design

Ghulam E Mustafa Abro¹, Bazgha Jabeen¹, Abdul Manan¹

Abstract:

There are several autonomous vehicles such that unmanned aerial vehicle (UAV), unmanned ground vehicle (UGV) and unmanned under-water vehicle (UUV). All these vehicles are proposed earlier for several applications. Researchers are still engaged in carrying out their research on hovercraft because of its hovering operation on land, water and ice. Moreover, due to this operation it has been significantly used in transporting the heavy loads from one place to another. Looking over its stability, power and size requirements, this paper proposes the stabilization of non-holonomic three degree of freedom (DOF) hovercraft using robust regulation and pole placement (RST) control design. This paper suggests dynamic controller design to stabilize the parameters of proposed prototype model of hovercraft. This control scheme enables our prototype to execute various tasks in dull, difficult, dangerous and dirty conditions. The paper proposes the Simulink based simulations to verify the results along with the validation with hardware results.

Keywords: Non-holonomic, air cushion vehicle, dynamically controlling, RST (Regulation, Pole Placement & Tracking)

1. Introduction

The term ‘under-actuated’ or ‘non-holonomic vehicles’ both are same and are defined as an autonomous system that have a smaller number of actuators as compared to the degree of freedom. The paper addresses the hovering state problem of non-holonomic three degree of freedom hovercraft. At this state the number of forces and all torques should converge to zero as soon as possible so that the hovercraft can continuously hover at the surface. The discussed prototype in this paper is non-holonomic in nature because it has fewer control inputs than the degree of freedom. Its control inputs are thrust forces along yaw moment, surge direction while its degree of freedom is in x, y and in the mid of these axis.

In the proposed non-holonomic hovercraft, the most prominent problem is to develop a particular control scheme. This scheme may be further responsible to stabilize the proposed non-holonomic hovercraft as it is not satisfying the Roger Brockett’s condition [1] of feedback control law that asymptotically stabilizing an equilibrium for proposed non-linear mechatronic system [2] and this is because

of the sway that is produced indirectly by actuators. Although this is one of the problems of non-holonomic structures, one may find several control designs in order to control and stabilize the position, velocity and torque parameters of hovercraft model [3]. One may find various controller schemes so that some of them are proposed in order to analyse the driving operation of an under-actuated hovercraft on particularly trajectory [4] [5] in a smooth way using backstepping technique. Moreover, some have proposed continuous time varying tracking controller for non-holonomic surface vessel [6] and some focuses on both trajectory tracking and path planning [7] in order to operate the vehicle on provided reference trajectory. After a brief study of such non-holonomic structures one may get an idea of several control designs that have been implemented on wheeled mobile robots [8]. There are various actuated systems such that under, over and fully actuated systems but underactuated systems are difficult to stabilize. In this regard several control techniques like sliding mode controller (SMC) and dual proportional integral derivative (D-PID) had been proposed for controlling the two wheels of wheeled

¹ Department of Electronic Engineering Hamdard University
Corresponding Author: Mustafaabro@hamdard.edu.pk

mobile robots (WMR) [2]. The most popular classical method suggested for non-holonomic structures is Regulation, pole-placement technique (RST) [9]. This paper proposes RST technique in order to analyse the hovering state of proposed non-holonomic hovercraft model at water and other surfaces.

It is obvious that any system's response may be affected by the external disturbances and for that purpose a non-linear observer technique [10] can be used. This technique not only estimates the external disturbance but also provide a way to reduce the disturbance error as well [11]. Furthermore, in our case these disturbances may vary frequently and are an obviously insufficient for robust stabilization. In order to reduce the effect of such disturbances one can use the estimators for dynamic coefficients (hydro-dynamic) [12] [13] using smooth projections. Nowadays, researcher prefers to implement hybrid control schemes in order to minimize the cons and maximize the pros. such that fuzzy based PID schemes [14]. These hybrid schemes can guarantee the stability as well as the bounded position error [15] but one may still face the singularity issues. After brief study of different algorithms it has been concluded that the machine learning based algorithms can eliminate this problem [16].



Fig. 1: Hovercraft CAD structure prototype and final

The main focus has been set on the deployment of an electronic circuit that can drive the proposed prototype precisely [17] as shown in figure 1. Moreover, in designing non-holonomic hovercraft the material of carbon fibre has been used in order to have less weight structure [18]. In all techniques proportional integral derivative (PID) is the easiest technique to implement and one may use fuzzy based PID technique to get much better results on such non-holonomic control system [19]. The proposed modelling and controlling work has been focused on hovercraft

because of its significance in transporting heavy payload from one place to another by just calculating and controlling the inputs [20]. One may look for various control algorithms to stabilize any desired system but one should also look for the advantages as well as disadvantages of these techniques.

Discussing proportional integral derivative controller (PID), it is easy to implement and stabilize the system, whereas it may generate non-suitable settling time and may also amplify noise frequency in the proposed plant. Linear quadratic regulator controller (LQR) is proposed at the times to model the system in the presence of any external noise i.e. gaussian white noise. This controller may be problematic when the dimension of the system state is larger and this problem is more difficult to solve because it is no longer separable. In addition to this, one may study sliding mode control (SMC) [2] that has an ability to stabilize even a non-linear system which cannot be stabilized by continuous state feedback laws, but the only problem with it is its implementation i.e. actuators had to cope with the high frequency control actions that could produce premature wear and tear. Moreover, one also proposes the back stepping control design for autonomous vehicles because it is implemented through chain of integrators while produces some states of the system as virtual inputs even though it has no any effect on system.

2. Equation of motion

On a two-dimensional plane, the movement of hovercraft can be illustrated as in figure 2. The proposed model has two thrust propellers for the manuevability in 03 directions. This basically generates two forces as F_x and F_y along with the orientation (x, y, θ) of the hovercraft.

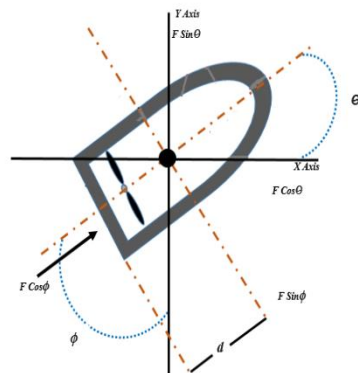


Fig. 2: Two-dimensional diagram for hovercraft model

Considering the above x-y plane, forces and observing the turning effect applied to hovercraft this paper presents the major six equations as mentioned below:

$$\begin{aligned} x &= u & 1.1 \\ y &= v & 1.2 \\ \theta &= r & 1.3 \end{aligned}$$

Whereas, their derivatives are, as mentioned below:

$$u = \frac{F\cos\theta\cos\theta - F\sin\theta\cos\theta - bu}{m} \quad 1.4$$

$$v = \frac{F\cos\theta\cos\theta + F\sin\theta\cos\theta - bv}{m} \quad 1.5$$

$$r = \frac{dF\sin\theta - br}{I} \quad 1.6$$

Hence the state space model can be developed using these six equations as shown below:

$$\begin{bmatrix} \dot{x} \\ \dot{y} \\ \dot{\theta} \\ \dot{u} \\ \dot{v} \\ \dot{r} \end{bmatrix} = \begin{bmatrix} 0 & 0 & 0 & 1 & 0 & 0 \\ 0 & 0 & 0 & 0 & 1 & 0 \\ 0 & 0 & 0 & 0 & 0 & 1 \\ 0 & 0 & 0 & -b/m & 0 & 0 \\ 0 & 0 & 0 & 0 & -b/m & 0 \\ 0 & 0 & 0 & 0 & 0 & -b\theta/l \end{bmatrix} \begin{bmatrix} x \\ y \\ \theta \\ u \\ v \\ r \end{bmatrix} + \begin{bmatrix} 0 & 0 \\ 0 & 0 \\ 0 & 0 \\ 1/m & 0 \\ 0 & 1/m \\ 0 & d/l \end{bmatrix} [Fx] \quad 1.7$$

$$C = [1 1 1 0 0 0] \quad 1.8$$

$$D = [0 0 0] \quad 1.9$$

In the above equations the u , v are the linear velocities and r as angular velocity. Moreover, the b_v , b_u are the co-efficient of linear frictional force and b_r or $b\theta$ is the co-efficient of angular frictional force. In the state space matrix the m is the mass and l is given as the length of hovercraft respectively.

3. Control design

In order to get an optimal desired response from an actual response the RST controller has been proposed. It is obvious that any control system will never work for the same as it had been performing initially because of the variation in several parameters. This variation may occur due to several reasons such that temperature pressure conditions or simply by external

disturbance (noise). Hence, one should look forward for a control design that may work on adaptive self-tuning of control systems. This paper proposes the technique named as regulation, pole-placement and tracking (RST) control design that is nothing but the placement of poles at right location.

RST or pole placement technique is the most widespread methodology used for advancing the control systems. Furthermore, if someone places feed forward controller along with feedback controller in order to manipulate the input in digital domain as well as reduces the noise or external disturbance, such technique is known as RST technique. The controller is based on the resolution of a Diophantine equation. In this heading, RST controller design is presented for the stabilization of non-holonomic hovercraft. Since RST technique is applied on discrete model hence the state space model will be turned into z-domain using the basic mathematics.

The transfer function of known system is,

$$G_p(q) = \frac{B(q)}{A(q)} \quad 2.0$$

Whereas the desired transfer function has been illustrated as,

$$G_m(q) = \frac{B_m(q)}{A_m(q)} \quad 2.1$$

RST based control algorithm provides fine results in stabilization the key response such that translational and rotational movement of hovercraft. By knowing the poles and zeros from the definition of transfer function paper proposes the below calculation and proposes the Diophantine equation:

$$Ru(t) = Tu_c(t) - Sy(t) \quad 2.2$$

Replacing S=T we get,

$$u(t) = \frac{T}{R}(u_c(t) - y(t)) = \frac{T}{R}(e(t)) \quad 2.3$$

Equation 2.3 represents the control law for controlling the desired parameters i.e., u , v and r (translational and angular velocities).

4. Simulation Results

Beneath this heading, one may look into the simulated control algorithm for non-holonomic hovercraft model using regulation and pole placement (RST) technique as illustrated in the figure 3.

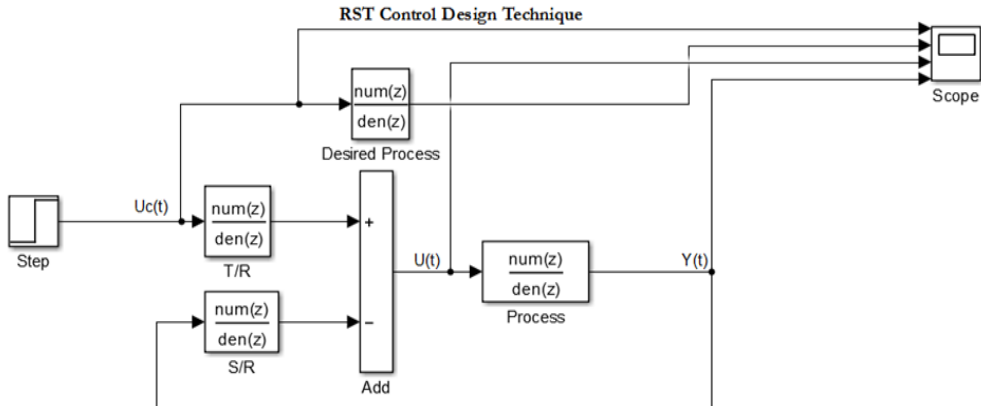


Fig. 3: Close loop (RST) based Control Diagram

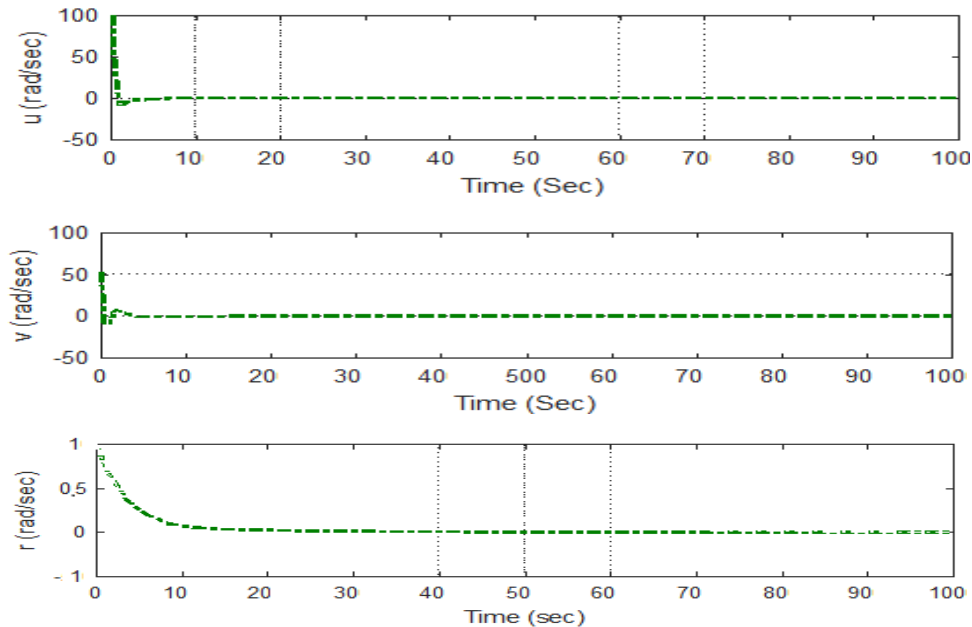


Fig. 4: Hovering state velocities u , v and r of proposed hovercraft

In the hovering state there would be two translational velocities and one rotational velocity namely u , v and r . The proposed RST control algorithm is designed to stabilize these velocities and converges it to zero state so that the hovercraft may continuously hover on sea or any other surface.

The simulation results for all velocities are shown in figure 4. Moreover the torque (turning effect) produced during the rotational maneuverability has been simulated at $\tau=0$, 0.5 and 1 as illustrated in figure 5.

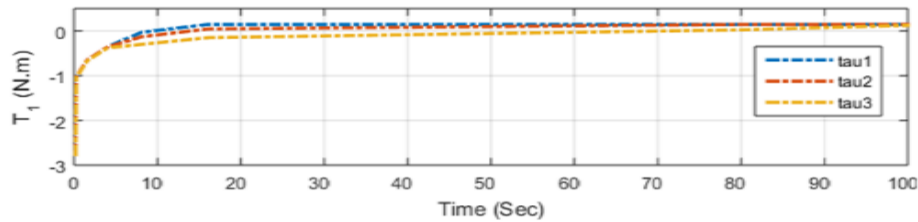


Fig. 5: The torque produced at different τ values

The feedback mechanism along with proposed control design shares the error

being occurred while covering distance in x y and in the mid of these axis while turning as illustrated in figure 6:

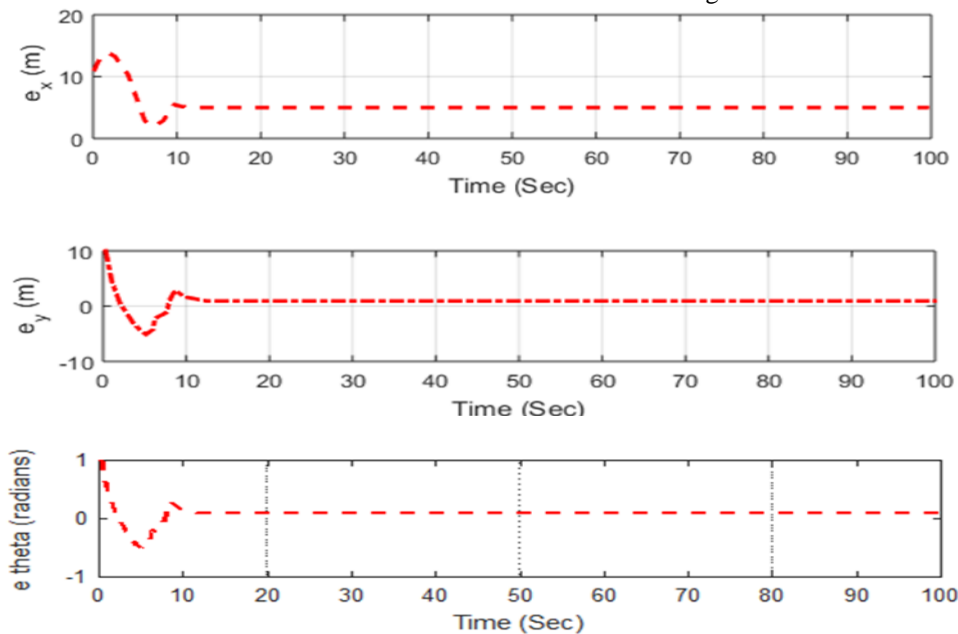


Fig. 6: The error signal produced with respect to u , v and r

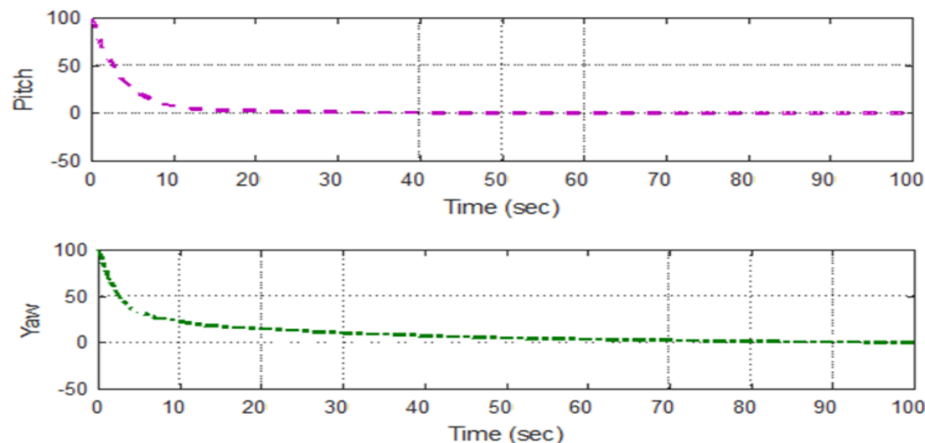


Fig. 7: Euler angles produced and simulated using Simulink

When proposed hovercraft is powered up, it will slightly go up from the front and at that moment the pitch is produced (rotation side to side) which is soon finished when the air in plenum settles or comes at equilibrium state. Moreover, rotation on vertical axis is known as yaw and this is produced when back fan along with rudder mechanism is powered up; the same settles at equilibrium state. It is noted that the rotation on front to back axis is known as roll that is not observed in this case as our ACV does not go in z-axis. The euler angles such that pitch and yaw are illustrated in figure 7.

5. Conclusion

In this paper robust RST controller is suggested to stabilize the non-holonomic 03 degree of freedom hovercraft model duly prepared in carbon fibre material. The technique not just controls the mathematically driven dynamics but also stabilizes the hovering state and three significant velocities and two Euler angles too. One may get all simulations and results being linked with each other. The best feature of the paper is the implementation of the algorithm at proposed model of nonholonomic hovercraft.

ACKNOWLEDGMENT

While working on this non-holonomic system from the first start to its final form, there were many of my mentors who came forward and encouraged on the completion of this technical paper. It is an immense honour to acknowledge here Dr. Valiuddin Professor at Hamdard Institute of Engineering and Technology HIET, Karachi and my co-authors of this paper for their invaluable encouragement and support. Whereas I am highly grateful to Gulbadin Khan Kakar research scholar at Polytechnic University Milan, Italy for his sincere involvement till last though he was out of country. I thank everyone once again for their kind support for bringing this piece of research to its final stage.

REFERENCES

- [1] R. W. Brockett, "Asymptotic stability and feedback stabilization," in *Differential Geometric Control Theory*. Basel, Switzerland: Birkhäuser Verlag, 1983, pp. 181–191.
- [2] M. Reyhanoglu, A. van der Schaft, N. H. McClamroch, and I. Kolmanovsky, "Dynamics and control of a class of underactuated mechanical systems," *IEEE Trans. Autom. Control*, vol. 44, no. 9, pp. 1663–1671, Sep. 1999.
- [3] I. Fantoni, R. Lozano, F. Mazenc, and K. Y. Pettersen, "Stabilization of a nonlinear underactuated hovercraft," in *Proc. 38th Conf. Decis. Control*, 1999, pp. 2533–2538.
- [4] A. P. Aguiar, L. Cremean, and J. P. Hespanha, "Position tracking for a nonlinear underactuated hovercraft: Controller design and experimental results," in *Proc. 42nd IEEE Conf. Decis. Control*, vol. 4, Dec. 2003, pp. 3858–3863.
- [5] H. K. Khalil, *Nonlinear Systems*. Upper Saddle River, NJ, USA: Prentice-Hall, 2002.
- [6] A. Behal, D. M. Dawson, W. E. Dixon, and Y. Fang, "Tracking and regulation control of an underactuated surface vessel with nonintegrable dynamics," *IEEE Trans. Autom. Control*, vol. 47, no. 3, pp. 495–500, Mar. 2002.
- [7] Xie, Wei, David Cabecinhas, Rita Cunha, and Carlos Silvestre. "Robust Motion Control of an Underactuated Hovercraft." *IEEE Transactions on Control Systems Technology* 99 (2018): 1-14.
- [8] A. Behal, D. M. Dawson, W. E. Dixon, and Y. Fang, "Tracking and regulation control of an underactuated surface vessel with nonintegrable dynamics," *IEEE Trans. Autom. Control*, vol. 47, no. 3, pp. 495–500, Mar. 2002
- [9] J. Alves *et al.*, "Vehicle and mission control of the DELFIM autonomous surface craft," in *Proc. 14th Medit. Conf. Control Automat.*, Jun. 2006, pp. 1–6
- [10] T. I. Fossen and J. P. Strand, "Passive nonlinear observer design for ships using Lyapunov methods: Full-scale experiments with a supply vessel," *Automatica*, vol. 35, no. 1, pp. 3–16, Jan. 1999.
- [11] K. D. Do, "Practical control of underactuated ships," *Ocean Eng.*, vol. 37, no. 13, pp. 1111–1119, 2010.
- [12] K. D. Do, Z. P. Jiang, and J. Pan, "Robust adaptive path following of underactuated ships," *Automatica*, vol. 40, no. 6, pp. 929–944, Jun. 2004.
- [13] K. D. Do and J. Pan, "Global robust adaptive path following of underactuated ships," *Automatica*, vol. 42, no. 10, pp. 1713–1722, 2006.
- [14] Safwan, Muhammad, Vali Uddin, and Muhammad Asif. "Nonholonomic mobile robot trajectory tracking using hybrid controller." *Mehran University Research Journal of Engineering & Technology* 35, no. 2 (2016): 161.
- [15] A. P. Aguiar, L. Cremean, and J. P. Hespanha, "Position tracking for a nonlinear underactuated hovercraft: controller design and experimental results," *Proceedings of the IEEE Conference on Decision and Control*, Maui, Hawaii, USA, Dec. 2003, pp. 3858–3863.
- [16] H. Sira-Ramirez, "Dynamic second-order sliding mode control of the hovercraft vessel," *IEEE Transactions on Control Systems Technology*, vol. 10, no. 6, pp. 860–865, Nov 2002.
- [17] Monitoring at neonatal intensive care units." In *Applied Sciences in Biomedical and Communication Technologies*, 2009. ISABEL 2009. 2nd International Symposium on, pp. 1-6. IEEE, 2009.
- [18] El-khatib, M. M., and W. M. Hussein. "Stabilization and Design of a Hovercraft Intelligent Fuzzy Controller." *International Journal of Engineering* 2, no. 12 (2013)
- [19] Ali, Zain Anwar, Daobo Wang, Muhammad Safwan, Wanyue Jiang, and Muhammad Shafiq. "Trajectory Tracking of a Nonholonomic Wheeled Mobile Robot Using Hybrid Controller." *International Journal of Modeling and Optimization* 6, no. 3 (2016): 136
- [20] "What is Motion Capture." 2016. [Online]. Available: <https://www.vicon.com/what-is-motion-capture>.

Effect of Tempering Temperature on the Properties of Martensitic Stainless Steel AISI-420

Iftikhar A. Channa¹, Aqeel Ahmed Shah¹, Shahid Hussain Abro¹, M. Ali Siddiqui¹, M. Mujahid¹, Ali Dad Chandio¹

Abstract:

Martensitic stainless steels are commercially significant materials owing to the remarkable properties they offer because of their martensitic structure during application. The paper aimed to investigate the effects of tempering temperature on mechanical properties and microstructure. Determination of carbide morphology was also included in the study to substantiate the results. This study used AISI 420 samples of 10 mm thickness, hardened at 1050°C and then subjected to tempering treatment at temperatures: 150°C, 250°C, 350°C, 450°C, 550°C and 650°C. Each sample was oil quenched after a soaking time of 25 minutes. Optical Microscopy and Scanning Electron Microscopy was conducted to examine the changes in the microstructure and the morphology of carbides. The results have shown that at various temperatures during tempering there is subsequent increase in toughness where hardness decreases and vice versa. Matrix of martensite contains some carbide precipitates. Due to Temper embrittlement occurring between 350°C-450°C, toughness has been decreased as a result of secondary hardening between the temperatures of 450°C-550°C, hardness has been increased drastically.

Keywords: Martensitic Stainless steel AISI 420, Tempering, microstructure, temper embrittlement, Secondary Hardening

1. Introduction

Martensitic Stainless Steel represents a portion of the 400 series of stainless steels and are essentially Fe-Cr-C alloys containing 12-13% Cr. Martensitic grades, due to the excellent mechanical properties, high wear resistance and moderate corrosion resistance, are used in various industrial components.

These wide variations of properties including strength, toughness and hardness values can be achieved through different heat treatments. [1]

Grade AISI 420 stainless steel possesses good ductility in annealed form notwithstanding the capability of being hardened up to 50 HRC. Optimum properties can be achieved with the control of the

¹ Department of Metallurgical Engineering, NED University of Engineering and Technology, Karachi, 75270, Pakistan

Corresponding Author: alidad@neduet.edu.pk

microstructure of these materials by means of austenitizing and tempering heat treatments [2]. An increase in austenitizing temperature results in more dissolution of carbides thus, Hardening treatment for this grade includes heating up to 1050°C, followed by quenching in oil or air which gives an optimum percentage of carbide distribution in the matrix resulting in high as-quenched hardness [3]. Tempering should be done at 150-370°C in order to get a wide variety of hardness values and mechanical properties. The tempering range of 425-550°C should be avoided [2]. The higher tempering temperatures will cause some precipitation of carbides with an alteration in mechanical properties [1]. In general, over the broad range of tempering temperatures, hardness decreases and toughness increases as the temperature is increased.

The prior heat treatment done on the steel has major influence on the final microstructure of AISI 420, which typically comprise of martensite, un-dissolved and/or re-precipitate carbides and retained austenite. The precipitation of carbides in the alloy during tempering is time dependent, which involves precipitation of M₃C followed by M₇C₃ and then M₂₃C₆ type alloy carbides [3][4]. The volume fraction and size of the carbide particles present in the steel and the amount of retained austenite play a major role in determining the hardness, strength and toughness of the steel [5]. The martensitic grades are generally susceptible to surface decarburization during heat treatment, if the furnace atmosphere is not properly controlled. However, with their high chromium content, they are relatively less susceptible than many of the low alloy steels.

2. Research Objective

The present research aims to investigate the behavior of Martensitic Stainless Steel, grade AISI-420, when it is subjected to a range of tempering temperatures. Considering the superior properties of stainless steels, it

becomes substantial to determine the influence of heat treatment processes on these steels. Tempering treatment can have considerable effects on the factors primarily focused in this study, namely:

- 1) Mechanical properties
- 2) Microstructure, and
- 3) Carbide Morphology

3. Experimental work

The chemical composition of the as-annealed sample was confirmed by R&D of Pakistan Steel mills. The composition of the sample is shown in the Table 1.

As illustrated in Figure 1, the samples were subjected to hardening at 1050°C for 25 minutes of soaking time in proportion to the dimensions of the samples (10mm x 10mm). The hardened samples were then tempered at 150, 250°C, 350°C, 450°C, 550°C and 650°C respectively for 25 minutes. All heat treatments were performed using PROTHERM furnace, Model 140/25.

Table I: Chemical composition of 420 Martensitic stainless steel

Element	Wt.%
C	0.34%
Si	0.40%
Mn	0.38%
P	0.03%
S	0.02%
Cr	12.67%
Ni	0.29%
Mo	0.08%

After tempering treatment, all the samples were investigated for their hardness with Rockwell hardness tester (Wolpert Tester Model N23AB) for all corresponding heat treatments as well as toughness was measured

through charpy impact test according to ASTM standard E-23. The steel samples were then grounded, polished and etched using Vilella's reagent (90ml ethanol, 10ml HCl and 2gm picric acid). Microstructure of these samples were studied at optical microscope as well as scanning electron microscope over and above, energy dispersive x-ray (EDX) to verify the precipitated types of carbide in the microstructure.

4. Results and Discussion

The hardness value of 92 HRB is measured from as-received sample which is in annealed condition and contains the carbides precipitates in fully ferritic matrix. After quenching from austenitizing temperature of 1050°C in oil medium, this hardness value is measured to be 58.5 HRC and the toughness as 7 J as shown in figure 1. This high hardness is attributed to the formation of lath martensitic structure, shown in figure 2. This as-quenched structure of fresh lath martensite is quite brittle and should be stress-relieved or tempered to restore some ductility. The little amount of carbides which was not dissolved at austenitizing temperature is also present in lath martensite matrix. The Ms Temperature of AISI 420 is found to be 380°C with carbon content of 0.34%.

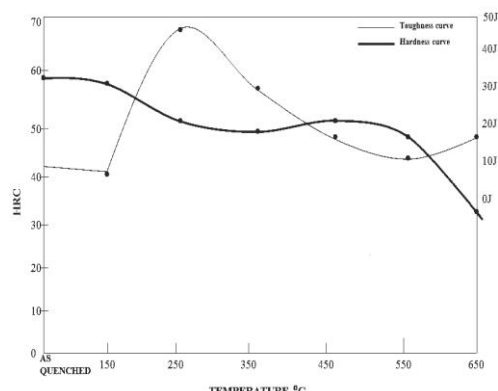


Fig 1:Hardness and toughness versus tempering temperature

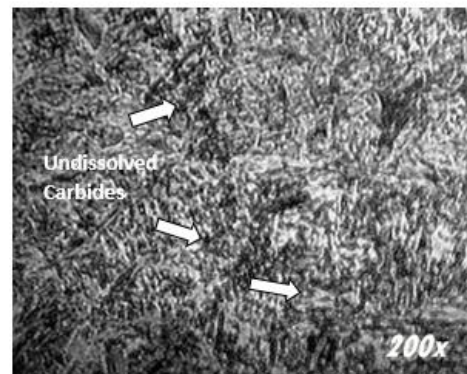


Fig 2:Optical micrograph of as quenched microstructure containing carbides in lath martensitic matrix.

4.1. Tempering at 150°C

By tempering up to 150°C, slight change in hardness and toughness with 58 HRC and 7J respectively as shown in figure 1, was observed because of the softening effect due to the depletion of carbon from martensite matrix is compensated by the precipitation of well-dispersed carbides but no increase in carbide precipitation occurs. According to Porter and Easterling [6], the carbide identified at this tempering temperature, as shown in figure 3, is the transition-carbide $\text{Fe}_{2.4}\text{C}$ of diameter 2nm due to some partial diffusion of carbon from supersaturated martensite.

4.2. Tempering at 250°C

At tempering temperature of 250°C, hardness of the steel drops to 52 HRC with significant increase in toughness of 42.5 J. During tempering between approximately 149°C and 316°C, a relaxation of the martensite structure occurs whereby the volumetric stresses associated with the formation of martensite upon quenching are relieved [7]. Volumetric stresses result in martensite structure decreasing in hardness

while according to figure 1, at the same temperature the high impact energy is due to the presence of retained austenite within the lath martensite, which is very soft as related to martensite, absorbing fracture energy. According to [8], tempering the hardened steel at 250°C facilitate precipitation of epsilon-carbides with restoration of distorted BCT structure by diffusing some trapped carbon into matrix. At this temperature some epsilon-carbides start transforming to Fe₃C [6].

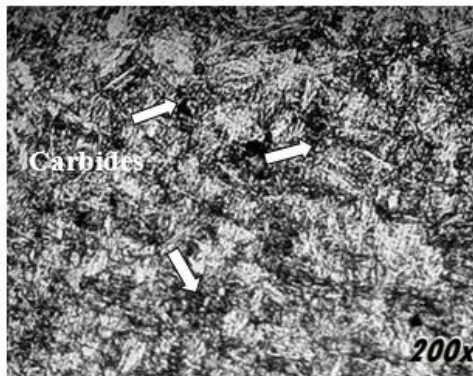


Fig 3: Optical micrograph hardened and tempered at 150°C. Microstructure contains carbides in lath martensitic matrix.

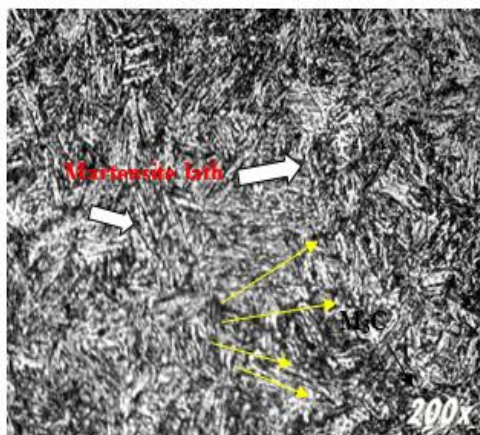


Fig 4: Optical micrograph hardened and tempered at 250°C. Microstructure containing carbides in lath martensitic matrix

4.3. Tempering at 350°C

Tempering at 350°C, the hardness then reached to 50 HRC and with decreases in toughness up to the value of 27.5 J as shown in figure 1. Decreases in hardness show that the relaxation of martensite persisted above 250°C while decrease in toughness is the result of tempered martensite embrittlement (TME) caused by the precipitation of carbides (Fe₃C) occurring at the expense of epsilon-carbide. Tempered martensite embrittlement is thought to be resulted from the combined effects of cementite precipitation on prior-austenite grain boundaries or inter lath boundaries and the segregation of impurities at prior-austenite grain boundaries. Besides if at grain boundary, the morphology of M₃C is predominantly more sheet-like and this would be the prime cause of low ductility in this temperature range. The transformation of retained austenite into ferrite and cementite also causes temper embrittlement [6].

4.4. Tempering at 450°C

The hardness as calculated at 450°C is 52.5 HRC with toughness 15 J as shown in fig.1. The increase in hardness in this range is attributed to secondary hardening phenomenon, which is due to the complex-forming carbides having noticeable effect on the retardation of softening and increase in hardness. It has been illustrated that the M₃C carbides are first detected after 200°C and these carbides remain until 450°C [9] but it was stated by Isfahany [4] that in the temperature range of 400-500°C, M₇C₃ starts to form within the martensitic laths. Above 350°C, the M₃C carbides progressively dissolve and M₇C₃ carbides start precipitating. A small amount of retained austenite is also remained as shown in figure 6.

4.5. Tempering at 550°C

With further increase in temperature at 550°C, the hardness drops to 51 HRC. This is due to softening phenomenon taking place when the M₇C₃ carbides start to coarsen which also caused drop off toughness to 12.5 J. Due to coarsening, M₇C₃ partially transform to M₂₃C₆ carbides [4] which is more stable form of carbides and remained at all temperature.

4.6. Tempering at 650°C

Here the hardness value is rapidly decreased to 36HRC and an increase in toughness occurs with 17 J. The softening occurs due to start of recrystallization above 600°C, as near to the sub-critical annealing range for AISI 420 that is to be 675-705°C [7]. After this temperature M₂₃C₆ carbide, occurring at the expense of M₇C₃, start to coarsen causing measurable decrement in hardness. The increase in toughness and decrease in hardness is due to recovery of meta stable martensitic phase but the lath structure remains [6] as shown in fig.8. Toughness should be considerably enhanced around 650-700°C temperature range but the ductility was restricted by the presence of coarse carbides, even however tempered martensite was present.



Fig 5:Optical micrograph hardened and tempered at 350°C. Microstructure contains M3C carbides in lath martensitic matrix

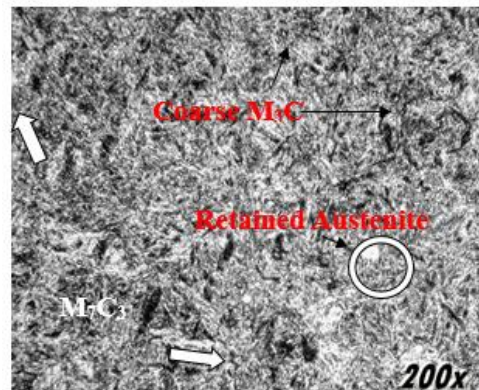


Fig 6:Optical micrograph hardened and tempered at 450°C. Microstructure contains carbides with retained austenite in lath martensitic matrix

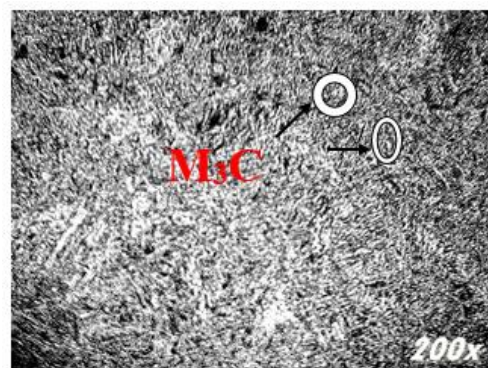


Fig 7:Optical micrograph hardened and tempered at 550°C. Microstructure containing carbides in lath martensitic matrix

5. Conclusion

An investigation of the effect of tempering temperature on AISI 420 Martensitic Stainless steel was conducted. After interpreting the results of this study on the basis of mechanical testing such as hardness and toughness and optical microscopy, the chief findings in this work are summarized as follows:

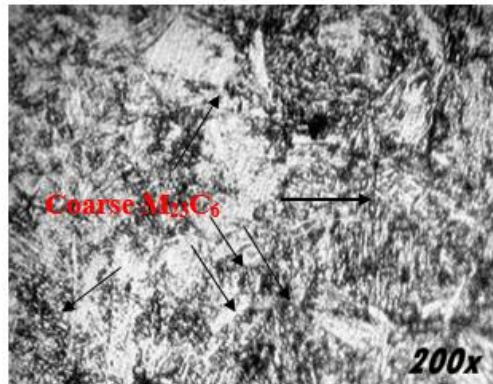


Fig 8: Optical micrograph hardened and tempered at 650°C. Microstructure containing carbides in lath martensitic matrix

1. Nice combination of mechanical properties of AISI 420 Martensitic stainless steel can be obtained by tempering near the range of 250°C with soaking time of 25 minutes as per dimension of 10x10mm sample.
2. Secondary hardening was obtained between the tempering temperatures of 400-500°C because of formation of secondary carbides M₇C₃. Hence this temperature range should be avoided if good toughness is required.
3. Decrease in toughness was observed between the tempering temperatures of 350-550°C.
4. The toughness again improved with rapid decreased in hardness of 36 HRC at 650°C due to start of recrystallization above 600°C, as the sub-critical annealing range for AISI 420 was found to be 675-705°C. At this temperature M₂₃C₆ carbides coarsened and this resulted in measurable decline in hardness.

ACKNOWLEDGEMENT

We would like to acknowledge Department of Metallurgical Engineering of NED University of Engineering and

Technology, Karachi for provision of facilities regarding this work and all the support and cooperation.

REFERENCES

- [1] Bhadeshia, H.K.D.H. and Honeycombe, R.W.K., Steels: Microstructure and Properties, Fourth Edition, Elsevier, 2017.
- [2] ASTM, AIME, Advances in the technology of Stainless Steel and Related Alloys, Philadelphia, 1965.
- [3] Isfahany, A. N., Saghafian, H. and Borhani, G., The effect of heat treatment on mechanical properties and corrosion behavior of AISI 420 martensitic stainless steel, Journal of Alloys and Compounds, 509, pp 3931–3936, 2011.
- [4] Stainless Steel – Grade 420 (UNS S42000), www.azom.com/article.aspx?ArticleID=972/, 2013
- [5] Xu, M.L., Secondary carbide dissolution and coarsening in 13% Cr martensitic stainless steel during austenitizing, Mechanical Engineering Dissertations, Paper 23, 2012.
- [6] ASM International, ASM Handbook Heat Treating Volume 4, 1990.
- [7] Rajasekhar, A., Reddy, G.M., Mohandas, T. and Murti, V.S.R., Influence of austenitising temperature on microstructure and mechanical properties of AISI 431 martensitic stainless-steel electron beam welds, Materials and Design, 2008.
- [8] Porter, D.A. and Easterling, K.E., Phase transformation in Metal and Alloys, Third Edition, Taylor and Francis group, 2009
- [9] Callari, I., Zanesco, M., Dabala, M., Brunelli, K. and Ramous, E., Investigation of microstructure and properties of a Ni-Mo martensitic stainless steel, Materials and Design, 29(1), pp 246–250, 2008.

0.7" Margin Top



Paper Formatting Guidelines

Title: 14^{pts} Bold**Author Name: 11^{pts} Bold***Affiliation: 11^{pts} Italic***Abstract:** Single Paragraph (Min: 150 – Max: 250 words)**Paper Length:** Formatted as guided (Min: 4,000 – Max: 8,000 words)**Font:** Times New Roman 10^{pts}**Font Color:** Black**Line Spacing:** 1.0 (single line space throughout the paper)**Indentation:** Justify**References & In-text Citations:** Follow the IEEE & Use EndNote X7 for In-text citations and Bibliography.**Headings: 12^{pts} Bold****1. 12^{pts} Bold****1.1. 11^{pts} Bold****1.1.1. 11^{pts} Bold Italic**

Margin Left
0.8"

Margin Right
0.5"

6.5"x10"*Page Size: 6.5" (Width) x 10" (Height)***Submission:** Formatted paper as guided can be submitted through our online submission system at <http://sjet.iba-suk.edu.pk>

1.9"
Margin Bottom

Publisher: Sukkur IBA Journal of Emerging Technologies (SJET)
Office of Research, Innovation & Commercialization – ORIC
Sukkur IBA University - Airport Road Sukkur-65200, Sindh Pakistan
Tel: (09271) 5644233 Fax: (092 71) 5804425 Email: sjet@iba-suk.edu.pk URL: sjet.iba-suk.edu.pk

Sukkur IBA Journal of Emerging Technologies



SUKKUR IBA UNIVERSITY
Merit - Quality - Excellence

SUKKUR IBA UNIVERSITY
Airport Road, Sukkur -65200
Sindh, Pakistan
Tel: +92-71-5644000
Email: sjet@iba-suk.edu.pk
URL: sjet.iba-suk.edu.pk